PNNL ARRA Report on the Development of Full-scale CFD Simulations of a Solid Sorbent Adsorber and Regenerator

Prepared by
Pacific Northwest National Laboratory
Richland, Washington 99352

In collaboration with Los Alamos National Laboratory, the National Energy Technology Laboratory, and Princeton University

Prepared for the
U.S. Department of Energy
National Energy Technology Laboratory

24 February 2012

Revision Log

Revision	Date	Revised By:	Description
0.1	17 Feb 2012	Avik Sarkar, Sebastien Dartevelle, DongMyung Suh, Xin Sun	Original draft
0.2	20 Feb 2012	Wenxiao Pan	Modified Introduction
0.3	21 Feb 2012	Avik Sarkar	Draft for Charity Plata
0.4	23 Feb 2012	Charity Plata	Technical Editing
1.0	24 Feb 2012	Xin Sun, Avik Sarkar	Final Version

Disclaimer

This report was prepared as an account of work sponsored by an agency of the United States Government. Neither the United States Government nor any agency thereof, nor any of their employees, makes any warranty, express or implied, or assumes any legal liability or responsibility for the accuracy, completeness, or usefulness of any information, apparatus, product, or process disclosed, or represents that its use would not infringe privately owned rights. Reference herein to any specific commercial product, process, or service by trade name, trademark, manufacturer, or otherwise does not necessarily constitute or imply its endorsement, recommendation, or favoring by the United States Government or any agency thereof. The views and opinions of authors expressed herein do not necessarily state or reflect those of the United States Government or any agency thereof.

Acknowledgement of Funding

This project was funded under the Carbon Capture Simulation Initiative under the following FWP's and contracts:

LANL - FE-101-002-FY10

PNNL - 60115

LLNL - FEW0180

LBNL - CSNW1130

NETL - RES-0004000.6.600.007.002

Table of Contents

List of Figures

Develop Full-scale CFD Simulations for Solid Sorbent Adsorber and Regenerator

List of Tables

Part I: Develop Full-scale CFD Simulations for Solid Sorbent Adsorber and Regenerator

Develop Full-scale CFD Simulations for Solid Sorbent Adsorber and Regenerator

Xin Sun[a] (chair), Sankaran Sundaresan[b] (co-chair), Sebastien Dartevelle[c], E. David Huckaby[d], Wenxiao Pan[a], Avik Sarkar[a], DongMyung Suh[a]

[a]Pacific Northwest National Laboratory, Richland, WA
[b]Chemical and Biological Engineering, Princeton University, Princeton, NJ
[c]Los Alamos National Laboratory, Los Alamos, NM
[d]National Energy Technology Laboratory, Morgantown, WV

Prepared by: Sebastien Dartevelle, Avik Sarkar, DongMyung Suh, Wenxiao Pan, Xin Sun

1. Introduction

CCSI aims to develop state-of-the-art computational modeling and simulation tools to accelerate the commercialization of carbon capture technologies from discovery to development and eventually the widespread deployment to hundreds of power plants through a partnership among national laboratories, industry, and academic institutions. The ultimate goal of the CCSI Toolset is to provide end users in industry with a comprehensive, integrated suite of scientifically validated models, delivering uncertainty quantification (UQ), optimization, risk analysis, and decision-making capabilities.

In this report, we present the models developed for two main units of carbon capture device: 1) the bubbling bed adsorber and 2) moving bed regenerator. They operate continuously to process the constant stream of flue gas generated by a power plant. In an adsorber, CO_2 is extracted from the exhaust flue gas by means of chemically active sorbent particles. The CO_2-saturated sorbent particles, which exit the adsorber, then are taken to the regenerator, wherein the CO_2 is released from the saturated particles. Subsequently, the refreshed sorbent particles are returned to the adsorber.

We set up a multiphase (solid and gas phase) flow model to capture the essential flow dynamics in these two units. The key input parameters and output variables are determined, and their responsive relation is established. In the present report, we summarize the concepts identified through computational studies. Our findings seek to provide science-based optimal designs that will reduce the time-to-design and troubleshoot real devices and processes. In addition, we provide a UQ analysis based on computational fluid dynamics (CFD) simulations. It begins by identifying input errors and uncertainty existing in the model and analyses how the effects of those propagate through the model, and how they affect the output of the model.

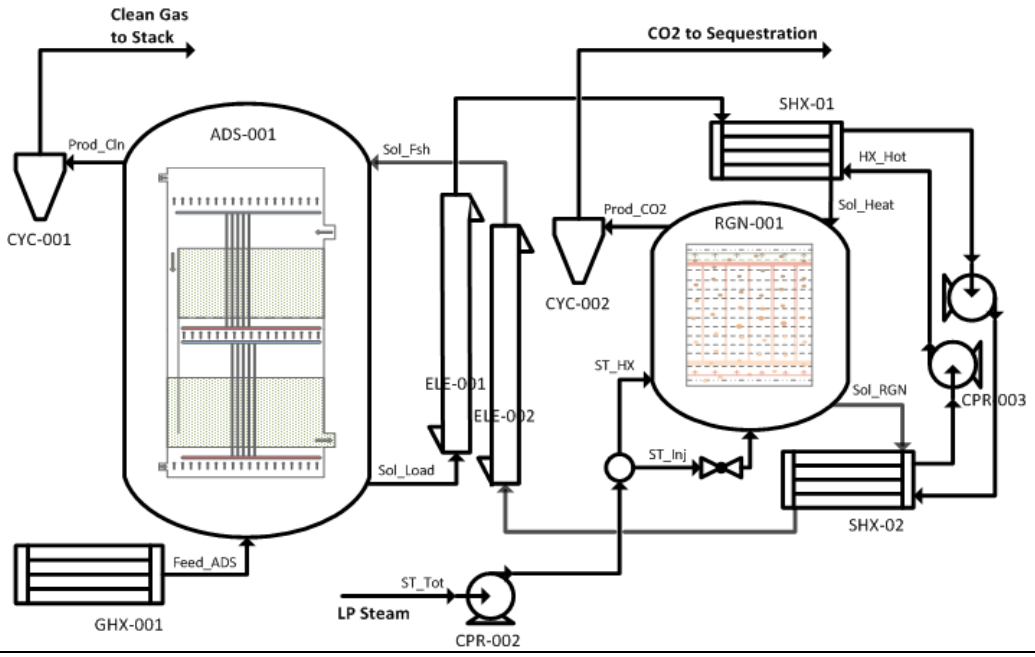

Figure 1.1. Schematic of the two-staged, counter-currently connected bubbling fluidized bed adsorber and moving bed regenerator.

2. Modeling the Adsorber

This section of the report presents a CFD analysis for the flow of solid particles and flue gas in the adsorber column as initially designed by Task-3 (Process Synthesis & Design). The goals of this work are: 1) demonstrate the modeling capabilities using multiphase flow simulations; 2) confirm whether the plant, as designed by Task-3, hydrodynamically behaves as expected; and, if not, 3) suggest (via CFD) further improvements in the initial design from Task-3. The information obtained from these simulations will be useful in optimizing the design of the full-scale adsorber trayed column, determining the most efficient operating conditions, and eventually predicting *in silico* performance efficiency of the adsorber system. Parametric studies are performed for varying operating conditions, e.g., flue gas inlet velocity, initial solid porosity, and solids inlet flow rate.

The present work focused on the flow dynamics of sorbent particles and flue gas on a single stage (tray) of the adsorber trayed column. The chemical reactions involved in CO_2 gas adsorption on sorbent particles are not included. Understanding the influence of operating and design conditions will assist in achieving the appropriate flow mode in the adsorber system. The amount of adsorption is expected to be strongly correlated to the mean residence time of solid sorbents and the available surface area of solid to the flue gas, i.e., particles that stay longer and are homogeneously scattered within a stage (no particle clustering) are more likely to be available for efficiently adsorbing CO_2 gas.

2.1. Adsorber design, geometry, boundary, and operating conditions

Schema of the adsorber column within the whole CO_2-capture plant system as provided by Task-3 is shown in Figure 1.1 (left, green, area: ADS-001). Figure 2.1 shows a schematic close-up of the adsorber two-stage column. Clean sorbent particles enter the adsorber column from the top, while hot flue gas comes in from the bottom of the column. The whole adsorber column is divided into two stages. Each is

separated by perforated trays, allowing flue gas to move upward. The whole adsorber column is crossed by cooling rods to cool down the flue gas and allow CO_2 adsorption on the solid particles. Eventually, at the bottom of the column, CO_2-enriched sorbent particles leave the system toward the regenerator column. As typical for a trayed column system, the top stage connects to the lower stage by a downcomer, allowing a continuous downward flow of particles to the lower next stage, where particles adsorb more CO_2 gas.

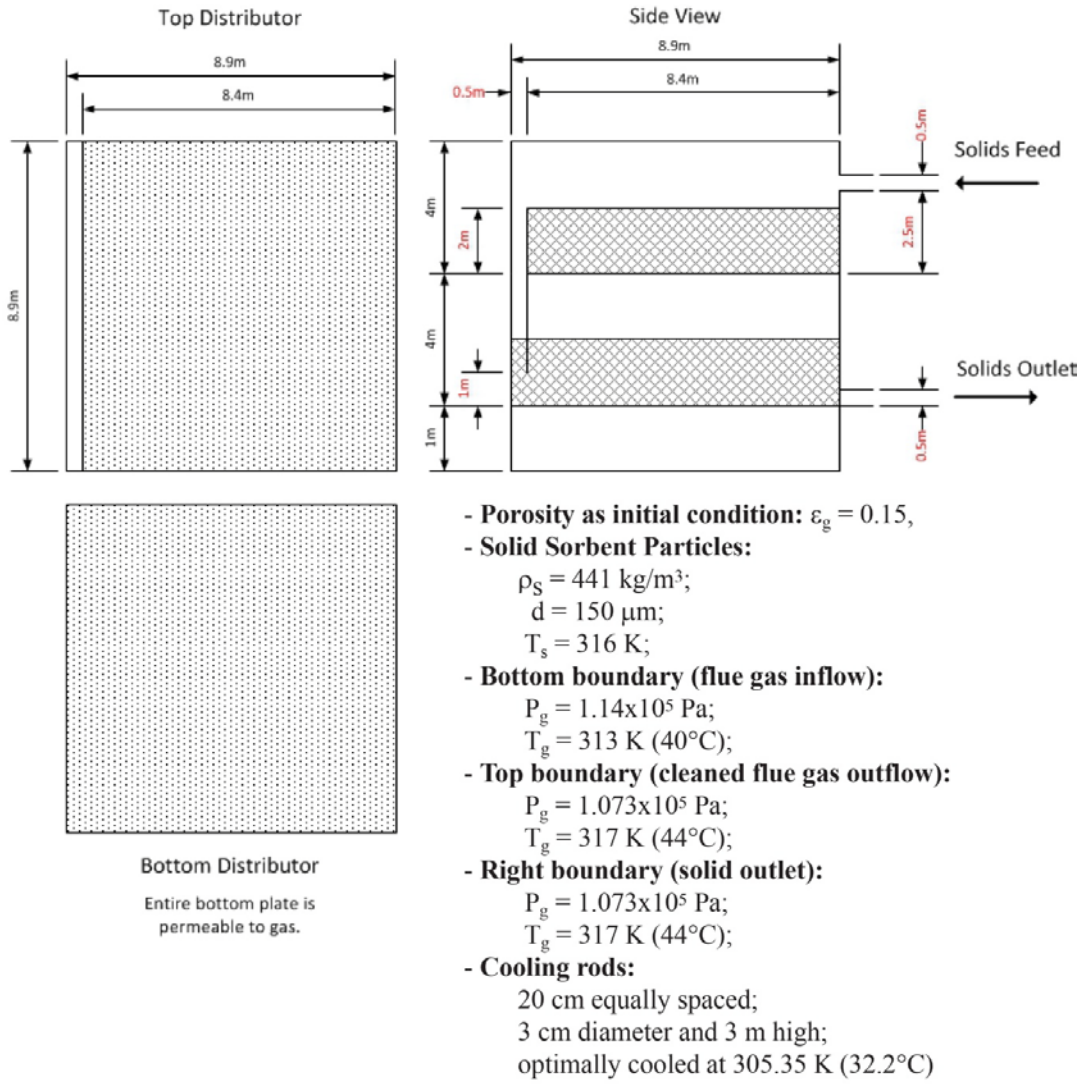

Figure 2.1. Adsorber two-stage trayed column. The areas in gray in the side-view sketch represent the cooling rods (Note: the initial design specified 2-m high cooling rods, which, at a later stage, was changed to 3-m high to increase the heat exchange efficiency and performance between the fluidized granular bed and the flue gas. This report will show that the change may not have been necessary).

The target of the full-scale CCSI adsorber is to process approximately 500-600 tons of sorbent per hour. To handle such flow rates, the characteristic dimensions of the adsorber are on the order of 10 m in all directions. The adsorber's efficiency, determined by the degree of adsorption by sorbent particles, is

strongly influenced by the residence time of the solids in the regenerator and by obtaining a homogenous fluidized system to maximize the solid particle surface areas (i.e., minimizing particles clustering).

The size of the adsorber column simulated with Multiphase Flow with Interphase eXchange (MFIX) code (from the initial Task-3 design) is 9 m × 9 m × 8 m. Schemata of the three-dimensional (3D) geometry are shown in Figures 2.2a, b, and c. Each stage (tray) has a height of 4 m with the first lower 3 meters occupied by vertical cooling rods. There are no cooling rods in the downcomer section. However, all simulations are performed in 3D Cartesian geometry with ad hoc filtered subgrid models over one tray (single stage).

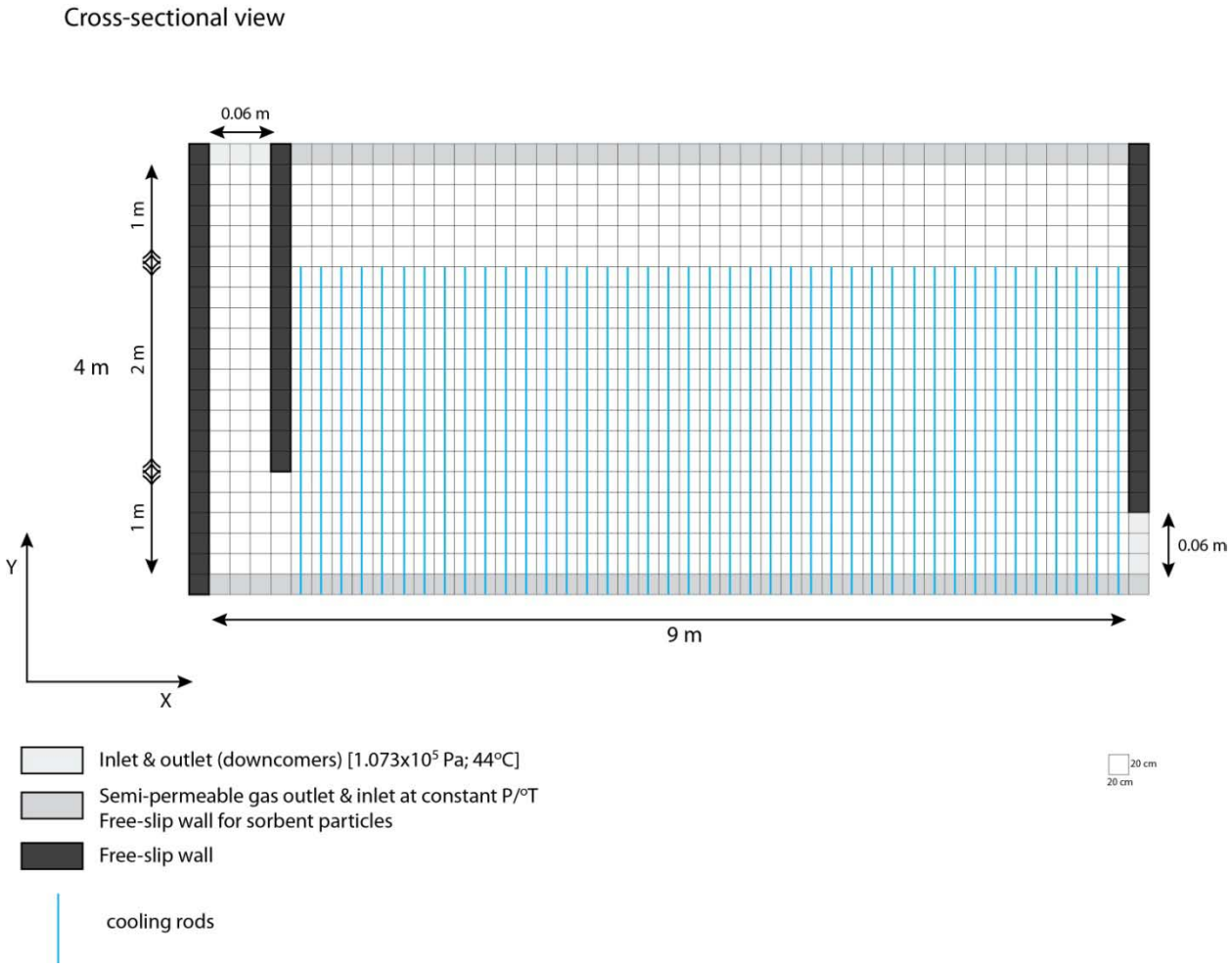

Figure 2.2a. Cross-sectional view of a single tray within the adsorber column as modeled by MFIX (compare with Fig. 2.1).

The boundary conditions used for the system are shown in Figure 2.3 (also see Figs. 2.2b and 2.2c). The solids inlet is modeled as a mass flow inlet (MI) on the left side at the top of the adsorber column. The gas that occupies the interstices between the entering solid particles is assigned an inlet velocity comparable to the solids inlet velocity (see Fig. 2.3). In MFIX, the corresponding solids outlet at the bottom (right side) of the regenerator is specified as a constant P/T mass outflow outlet (PO). The inlet for the flue gas is situated at the bottom of the adsorber column and set as MI.

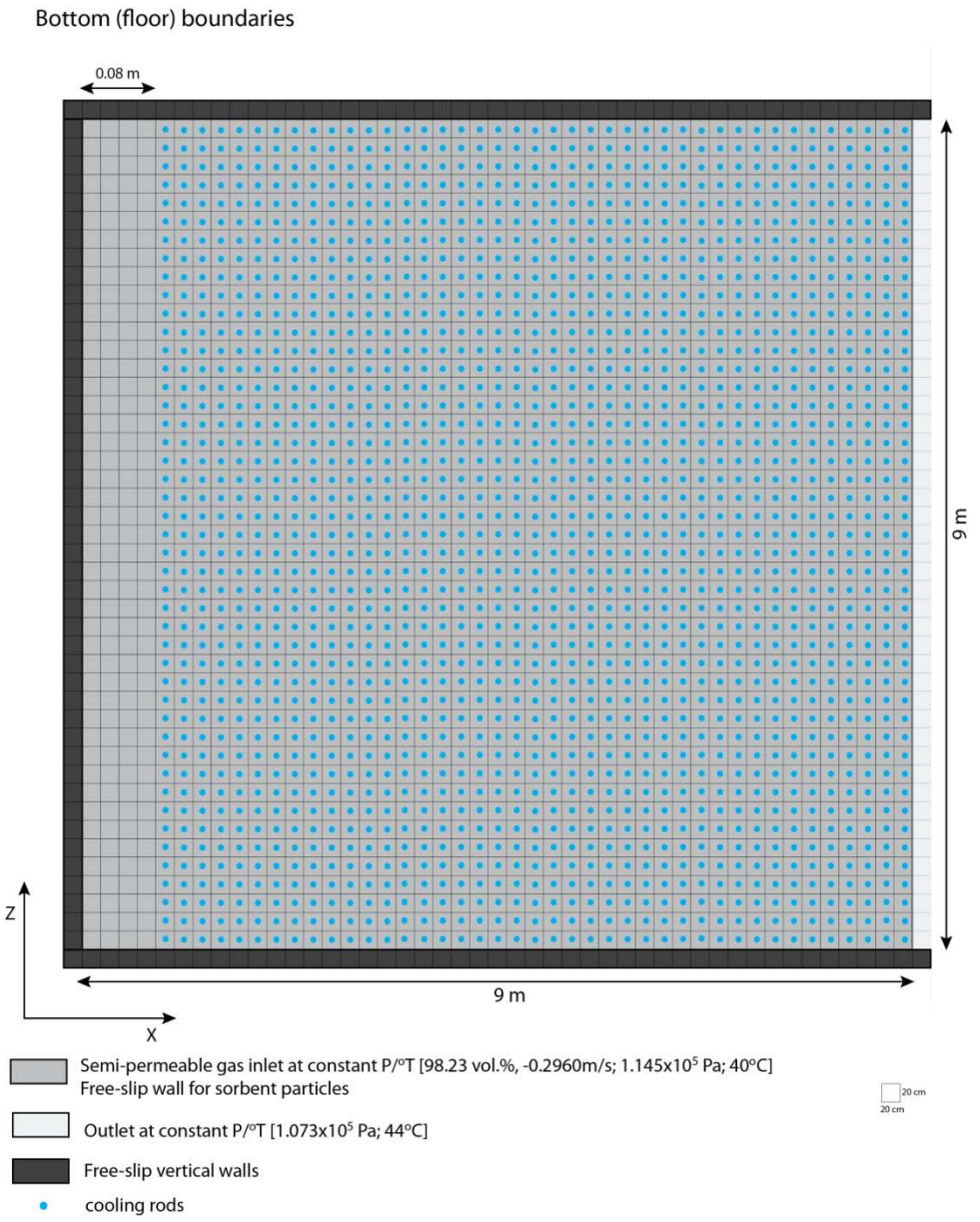

Figure 2.2b. Top view of the floor boundaries of a single tray within the adsorber column as modeled by MFIX.

This inlet mass flow rate for the flue gas is a controllable parameter, and is one of the parametric investigations in this work. The gas outlet is positioned at the top of the column and is modeled as constant PO in MFIX. To prevent sorbents from flowing out either at the bottom gas inlet or top gas outlet, the floor and roof are surrounded by semi-permeable membranes that only allow gases to pass through. Figure 2.3 summarizes the temperature and pressure initial and boundary conditions.

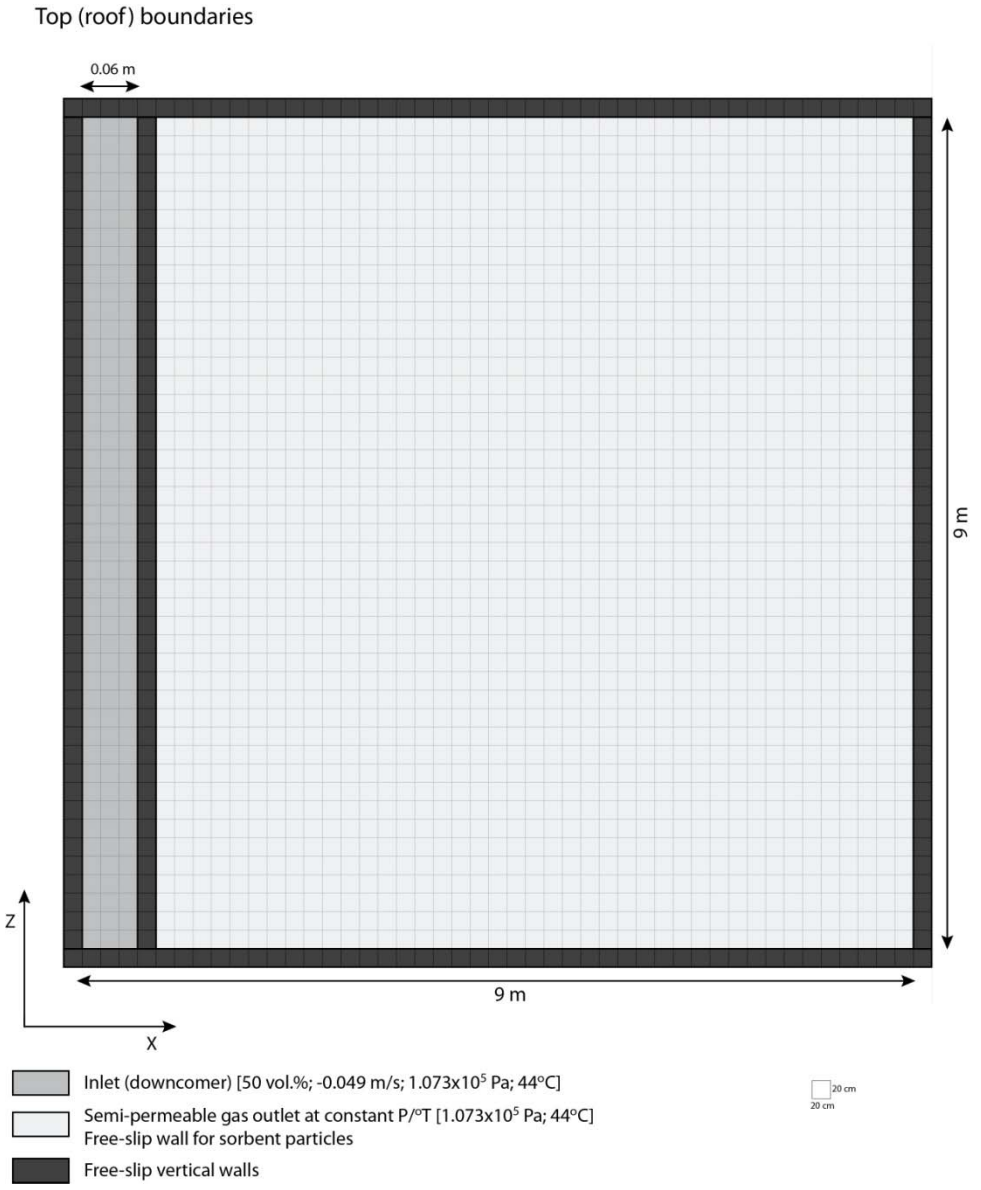

Figure 2.2c. Top view of the roof boundaries of a single tray within the adsorber column as modeled by MFIX.

Spatial discretization is composed of regular 3D cells, 20 cm in each direction. Hence, there are 45 cells in the X-direction (I) and Z-direction (K) and 20 cells in the vertical Y-direction (J). Given the coarseness of this Cartesian mesh, a filtered subgrid model was used for both stresses and drags (Igci et al. 2012).

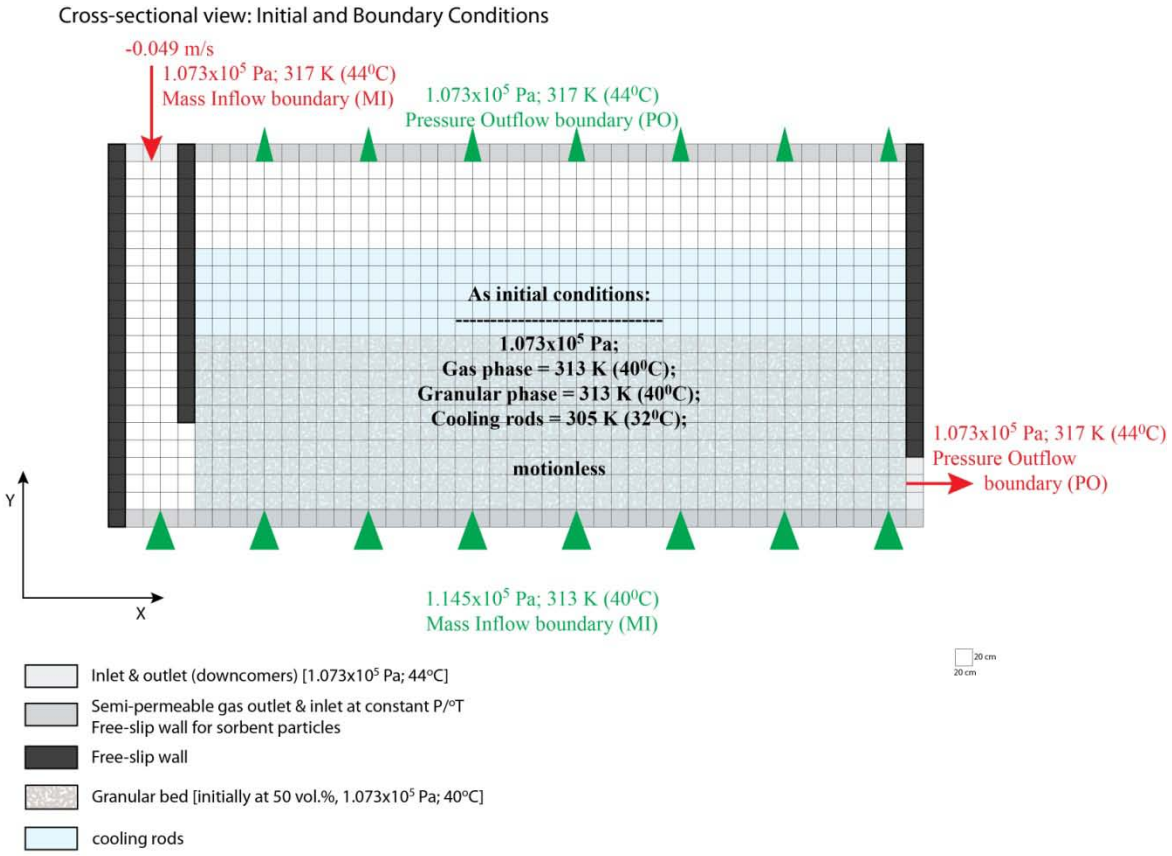

Figure 2.3. Cross-sectional view with boundary and initial conditions specified of a single tray within the adsorber column as modeled by MFIX. Notice that the mass influx of the flue gas at the bottom (in green) is not specified in this figure (it will be subject to discussion in this report).

An important feature of each stage of the adsorber trayed column is the presence of cooling rods that occupy the lower first 3 meter of each tray. These rods have a diameter of 3 cm, which, by all practical means, is too small to be simulated individually. Hence, the stage volume occupied by these rods will be modeled as a porous medium to reduce the available space for flowing through by flue gas and solid sorbents. Porosity in any Cartesian cell 20 cm × 20 cm × 20 cm in dimension is easily calculated by the volume occupied by a centered cylindrical rod within a given cell as shown by Figure 2.4.

The volume of Cartesian cell can be expressed as: $\delta x \cdot \delta y \cdot \delta z = 8x10^3$ cm^3, while the volume of one cylinder centered in that Cartesian-cell equals: $\pi \cdot r^2 \cdot \delta y = 141.37$ cm^3. As such, the constant porosity induced by the presence of a cooling rod can be expressed as: Vol.cylinder/Vol.cell = 1.767 vol.%. Practically speaking, this constant "porosity" within the whole cell is made of solid material with ρ = 995.7 kg/m^3 and T = 303.15 K (30°C). No momentum equation is solved for the cooling rod solids phase.

We also modified the MFIX code to allow energy to be exchanged between these "cooling rods" at constant temperature (305.35 K) and the rest of the flow field. Because of the volumetric presence of these cooling rods, Figure 2.5 shows the resulting volumes occupied by the flue gas and solid sorbent particles as initial conditions.

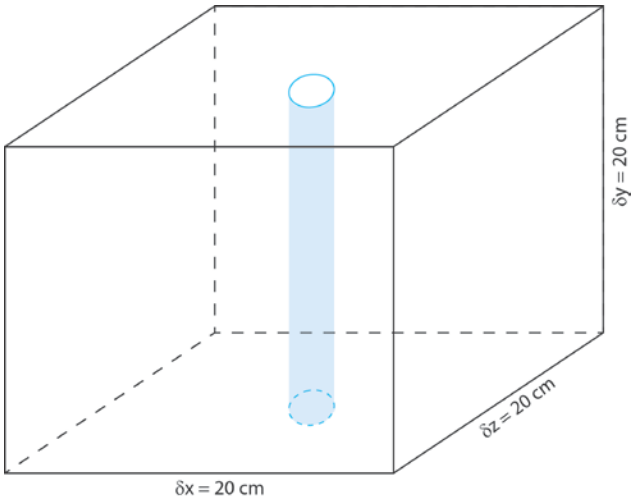

Figure 2.4. A single cooling rod in a Cartesian cell. The volume occupied by the cooling rod within a 20 cm × 20 cm × 20 cm cell is 1.767 vol.%.

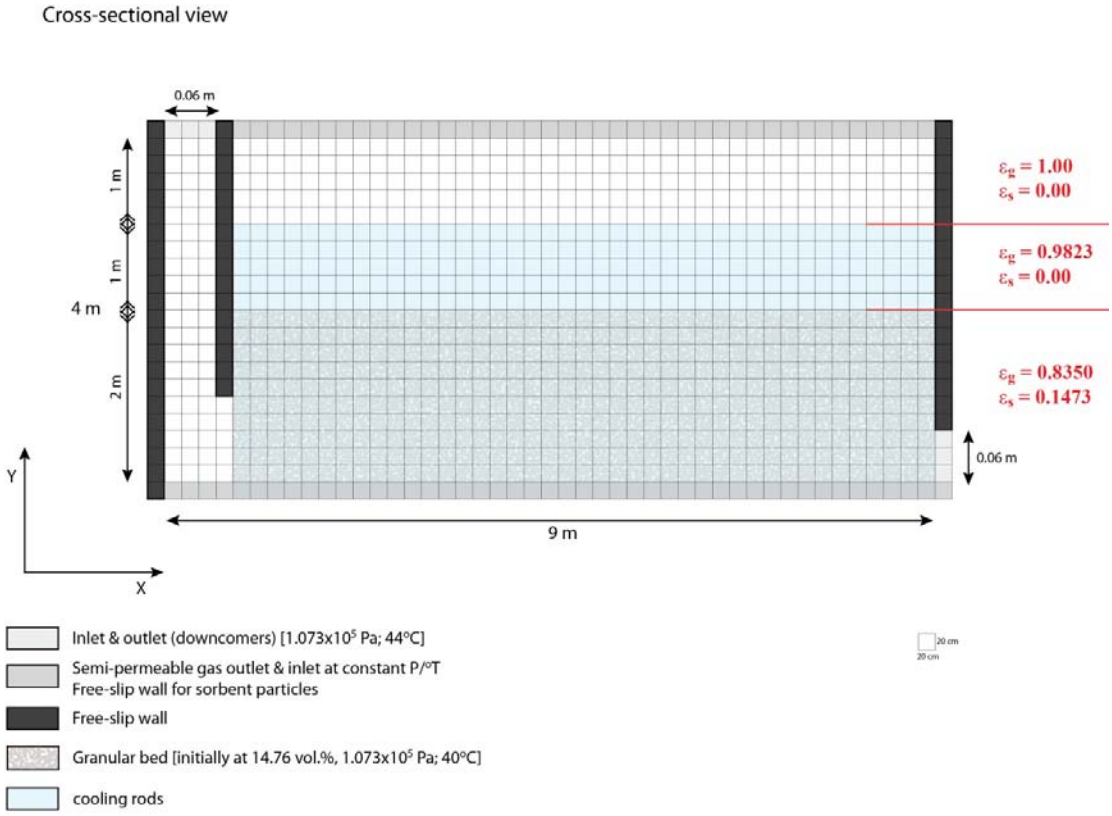

Figure 2.5. Cross-sectional view showing the impact of the cooling rods on the resulting porosity of the flue gas and solid sorbent particles as initial conditions within a single tray inside the adsorber column as modeled by MFIX.

2.2. Terminal velocity, minimum fluidization velocity, and mean residence time

Because Task-3 left the CFD team some degrees of freedom with respect to the fluidization speed of the flue gas at the bottom mass inflow boundary, it would be important to consider velocity scaling. For gas-particle multiphase flows, minimum fluidization velocity and terminal velocity are two important quantities to consider.

The minimum fluidization velocity, U_{mf}, is the upward superficial velocity of the gas when the weight of the particle bed is exactly balanced by the drag exerted by the gas on the particles. If the superficial gas velocity is increased beyond U_{mf}, the bed starts to fluidize. Knowing that the vertical speed of the flue gas ($V_{y,g}$) will be small enough to keep the Reynolds number low (i.e., $\mathrm{Re} = \frac{\rho_g V_{y,g} d_s}{\mu_g} \square 5$), one can calculate U_{mf} by:

$$U_{mf} = \frac{\left(\rho_s - \rho_g\right) g\, d_s^2}{150\,\mu_g} \cdot \frac{\phi_{s,mf}^3}{\left(1-\phi_{s,mf}\right)}, \tag{2.1}$$

where ρ_s (441 kg/m^3) and ρ_g (~1.127 kg/m^3) are the solids and gas densities, d_s is the particle diameter (150 μm), and μ_g is the gas viscosity (~1.98x10^{-5} kg/m·s). The solids volume fraction at the point of minimum fluidization is denoted by $\phi_{s,mf}$ and typically lies between 0.40-0.45. Fluidized beds are typically operated at 30·U_{mf}, sometimes going up to 100·U_{mf}. From this, the value of U_{mf} is ~0.0061 m/s (or 0.61 cm/s) at $\phi_{s,mf}$ ~0.46391. In this section, the effect of inlet flue gas superficial velocity, $V_{y,g}$, also will be investigated.

Another important physical property of the particle is the terminal velocity (*Vt*), which is the constant falling speed of a particle when the downward force of gravity equals the upward force of drag, causing the net force on the object to be zero and resulting in no net acceleration. *Vt* is given by Stokes' law:

$$Vt = \frac{\left(\rho_s - \rho_g\right) g\, d_s^2}{18\,\mu_g}, \tag{2.2}$$

which is ~0.272 m/s for the particles under consideration in this report.

Finally, the last quantity of importance for this study is the mean particulate residence time at steady state given that the particles must remain long enough to maximize the CO_2 adsorption processes. If particles have a (too) short mean residence time in the adsorber column, the CO_2 will not have enough time to efficiently adsorb on the particles regardless of how the system is homogenously fluidized. The mean residence time, $\overline{t}_{res}$, is a function of the average mass flow of the particles and the size of the vessel. It can be calculated by (Levenspiel 1999):

$$\overline{t}_{res} = \frac{m_{holdup}}{\dot{Q}} = \frac{\left(\rho_s \cdot \phi_{s,avg}\right) V_{vessel}}{\dot{Q}}, \tag{2.3}$$

where m_{holdup} is the steady state particulate mass holdup, $\dot{Q}$ is the steady state particulate mass flow rate through the vessel, $\phi_{s,avg}$ is the average steady state solids volume fraction in the vessel, and V_{vessel} is the volume of the tray adsorber modeled (9 m × 9 m × 4 m = 324 m^3) or the volume optimally occupied by the particles in the adsorber. In the following simulations, we have not changed the particulate mass flow rate at the top inlet boundary as this was an imposed condition from Task-3. The inlet for fresh sorbent coming down from the top was 50% solid $V_{s,y}$ = -0.049 m/s and 50% gas $V_{g,y}$ = -0.049 m/s. Knowing that the surface area (*SA*) of the top inlet is 0.06 m x 9 m = 0.54 m^2, the particulate mass inflow rate at this top inlet can be easily inferred as:

$$\dot{Q}_{in} = (\rho_s \phi_s) \cdot SA \cdot V_{s,y} = 5.83 \ kg/s \quad (2.4)$$

Again, except for the last one, this value was unchanged for any simulation herein.

2.3. MFIX codes

MFIX codes are a set of multiphase-CFD FORTRAN codes from the MFIX project managed by the National Energy Technology Laboratory (NETL) and Oak Ridge National Laboratory (ORNL): http://www.mfix.org.

MFIX relies on the Implicit Multiphase Formalism in which each phase (i.e., gas and solid particles) is modeled as a continuum. It solves Navier-Stokes and energy partial differential equations (PDEs) for each phase with appropriate interfacial coupling between phases. All PDEs are solved with second-order accurate finite-volume scheme (SMART) using deferred correction methods (DCM). DCM allies the stability of a first-order method with the accurateness of a second-order scheme. MFIX is fully parallel capable and can work either in shared memory mode (it has embedded Open-MP codes), distributed memory mode, or hybrid (both SMP and DMP).

Multiphase turbulence is simulated with a subgrid model analog to the large eddy simulation (LES) approach used for single phase flow. A simple Smagorinsky LES model is used for the LES subgrid dissipation for the gas phase, while a new subgrid model for the solid (dispersed) phase is used, which properly accounts for microscopic-scale effects from the dispersed phase within the subgrid (Igci et al. 2012). This new dispersed phase subgrid model modifies the formulations of the solid filtered stress and gas-solid drag. At high solid particulate concentration (>50 vol.%), a visco-plastic model is used to model frictional contacts between particles.

2.4. Results

2.4.1. Simulation 59.92 kg/s

This simulation was based on initial and boundary conditions initially set by Task-3 (Process Synthesis & Design):

Initial granular bed porosity, ε_s = 0.50
Vertical speed of flue gas at bottom inlet, $V_{g,y}$ = 0.633 m/s (or 59.921 kg/s mass flux)

The mass flux of the flue gas of 59.921 kg/s is more than twice *Vt* and more than 100 times U_{mf}. Figure 2.6 shows the time sequence of this simulation. As the flow proceeds, the particles are pushed upward as a whole and eventually cluster on the roof of the tray. After a minute, Rayleigh-Taylor instabilities start to form on the roof. This situation, where the surface area of the particles is clearly reduced by the formation of particle clusters on the roof and most of the lower half of the tray is now unoccupied by particles, is to be avoided at all costs. Due to these instabilities, this simulation was terminated at 116 s.

2.4.2. Simulation 40.0 kg/s

After a few more iterations and trials,

Initial granular bed porosity, ε_s = 0.15
Vertical speed of flue gas at bottom inlet, $V_{g,y}$ = 0.395 m/s (or 40.0 kg/s mass flux)

As first trials, the flue gas vertical speed was lowered to a bit more than *Vt*, i.e., 0.296 m/s. This simulation showed promising results to such an extent that $V_{g,y}$ was eventually increased to 0.395 m/s (40 kg/s) or $64 \cdot U_{mf}$ to maximize the granular bed height as much as possible without any particle clustering. Figure 2.7 shows the time sequence of this 40 kg/s simulation.

In this simulation, nearly half of the tray height is occupied by a uniformly fluidized granular bed with little evidence of any particle clusters in space and time. The highest concentrations of solid materials are found at the bottom of the downcomer and never exceed 0.24 (see Figs. 2.8 and 2.9). Figure 2.8 shows the solid volumetric concentration distribution at 300 s in all the numerical cells of the computational domain. Interestingly, there are two volumetric concentration modes: one in the dilute part at 0.042 and the other, more important and pervasive in the domain, at 0.175. To identify the origin of the dilute mode, the flow was sampled at 300 s in the downcomer and within the main tray (without the downcomer area) as shown in Figure 2.9. For each part, a single dominant mode can be identified, i.e., a dominant mode at 0.175 for the tray, and a dilute mode at 0.042 for the downcommer, explained by the particles falling down from the top-inlet.

Figure 2.6 (59.92 kg/s) and Figure 2.7 (40.0 kg/s). Volumetric concentration of a solid (blue = no solid; red = more solid) taken at different times. The left side of a given figure depicts 3D cross-sectional views of the front, middle, and back panels. The right side shows the middle panel only. The glyph represents the velocity vector of the gas phase.

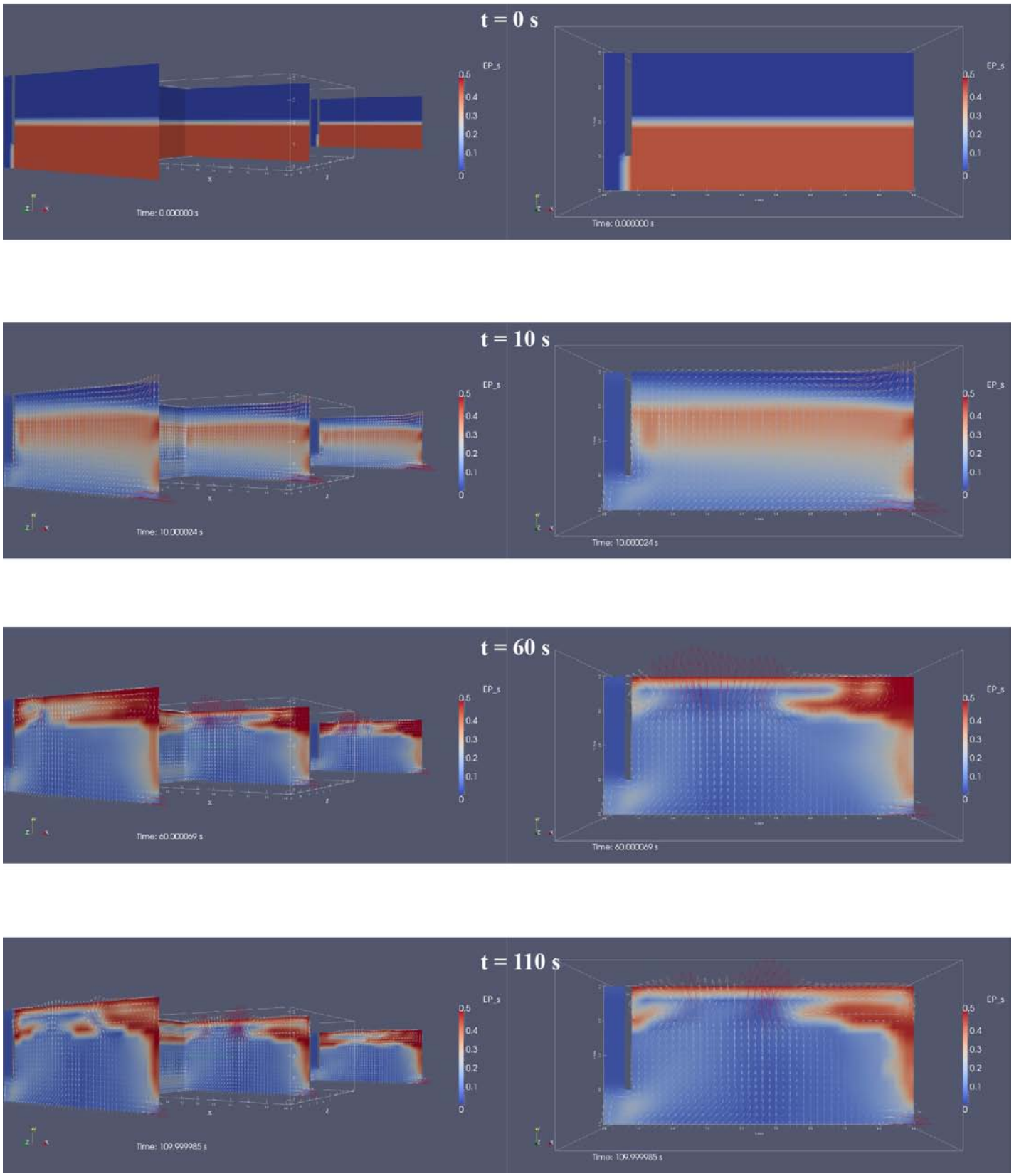
3D cross-sectional view
Centered planar cross-sectional view
t = 0 s
t = 10 s
t = 60 s
t = 110 s
EP_s
0.5
0.4
0.3
0.2
0.1
0
Time: 0.000000 s
Time: 10.000024 s
Time: 60.000069 s
Time: 109.999985 s

Figure 2.6.

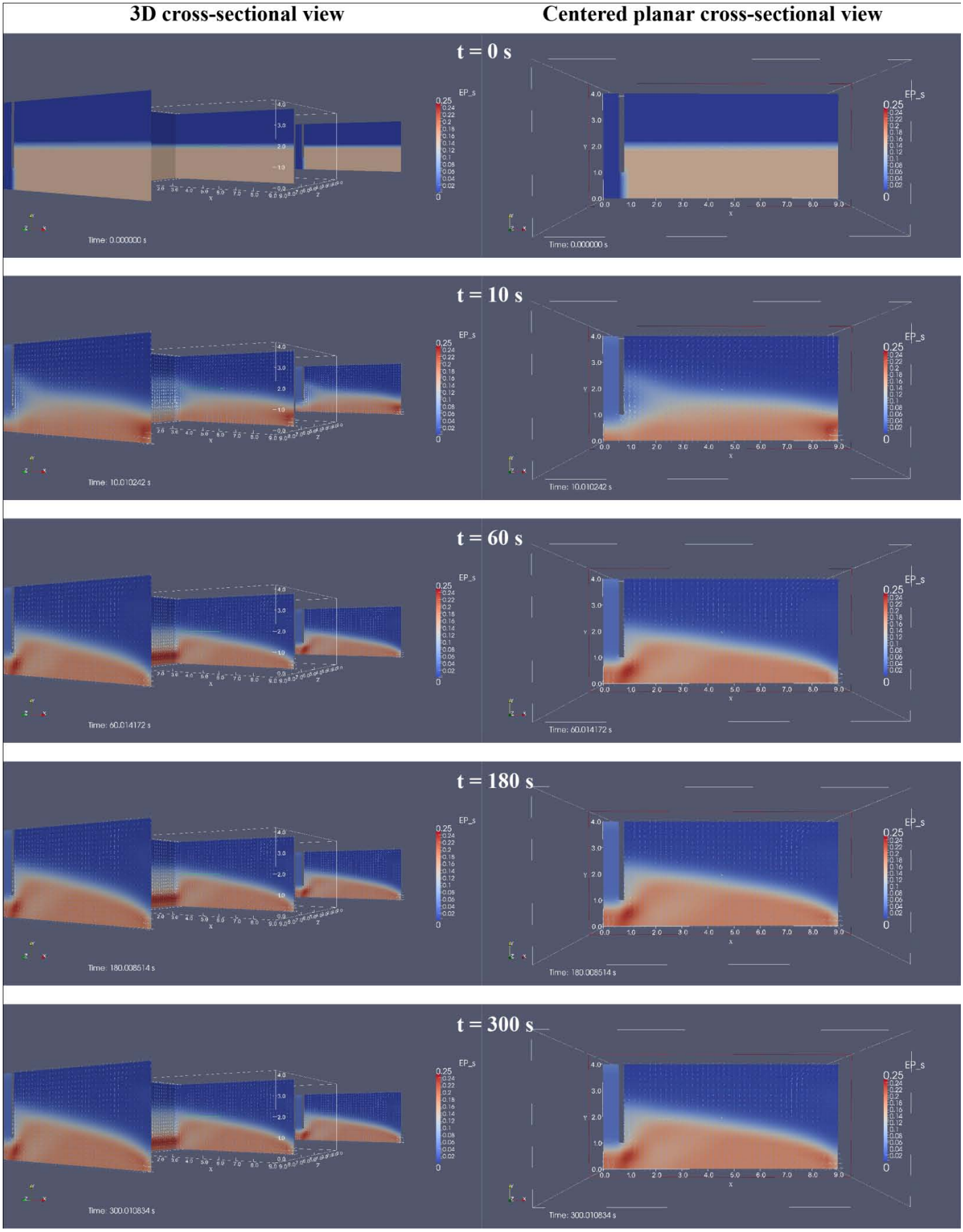
3D cross-sectional view
Centered planar cross-sectional view
t = 0 s
t = 10 s
t = 60 s
t = 180 s
t = 300 s
EP_s
Time: 0.000000 s
Time: 10.010242 s
Time: 60.014172 s
Time: 180.008514 s
Time: 300.010834 s

Figure 2.7.

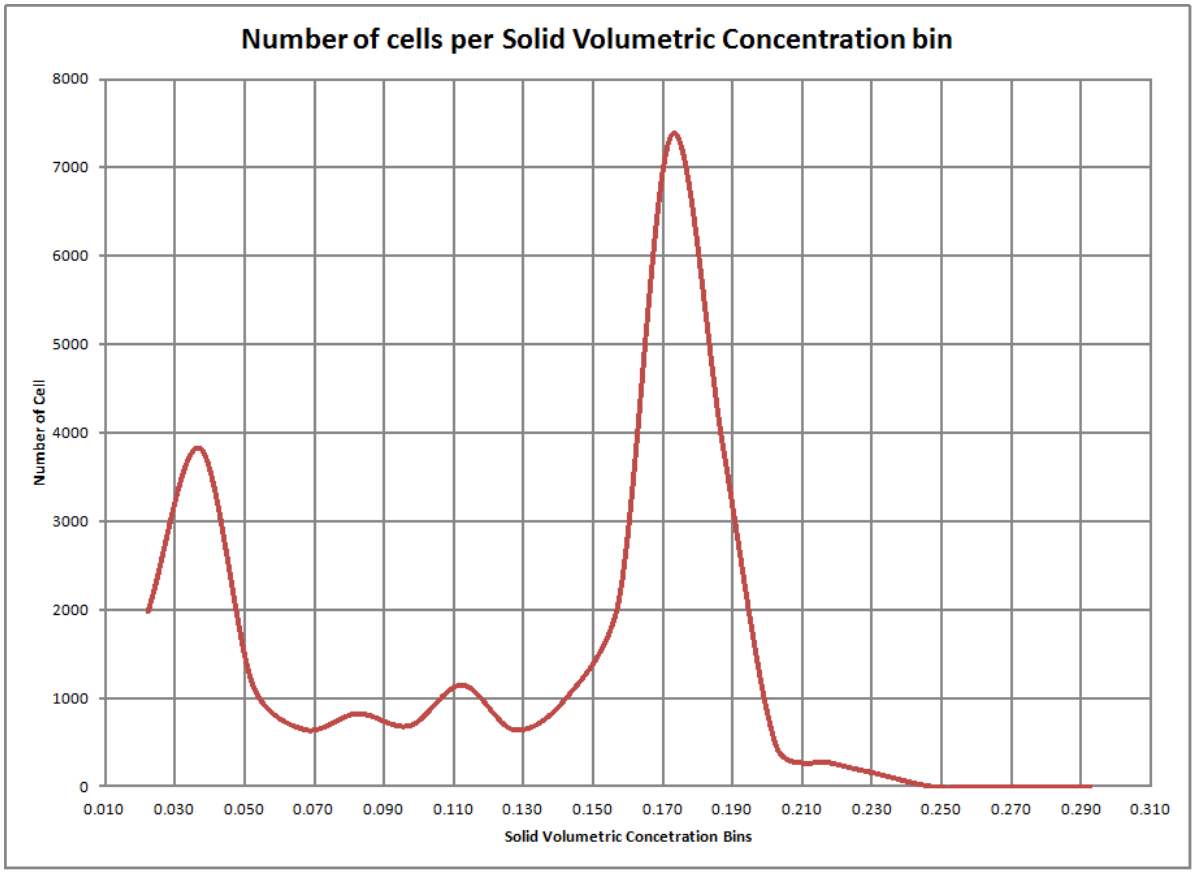

Figure 2.8. Histogram distribution of the solid volumetric concentration in the whole domain at 300 s. Note the two solid volumetric concentration modes at 0.175 (17.5 vol.%) and 0.042 (4.2 vol.%). This distribution of solid volumetric concentration does not change once steady state is reached at ~30 s.

From Figure 2.10, one can infer the particulate mass outflow at steady state knowing that the surface area (*SA*) of this outflow boundary is 0.06 m × 9 m = 0.54 m^2,

$$\dot{Q}_{out} = \left(\rho_s \phi_s\right) \cdot SA \cdot V_{s,y} = 3.35 \ {}^{kg}\!/\!_{s}\ , \tag{2.5}$$

which is significantly less than the imposed particulate mass inflow (5.83 kg/s).

Thus, the average particulate mass flux throughout the vessel is, on average, at steady state, ~4.59 kg/s, and the mean residence time of solid material in the vessel is:

$$\bar{t}_{res} = \frac{\left(\rho_s \cdot \phi_{s,avg}\right) V_{vessel}}{\dot{Q}} \approx \frac{\left(441 \cdot 0.17\right) \cdot 162}{4.59} = 2646 \text{ s} = 44.1 \text{ min}\ , \tag{2.6}$$

where we took only half the of the available vessel height because the fluidized granular bed occupies an optimal height of only ± 2 m as shown in Figure 2.7 and Figure 2.11. This residence time is a bit more than what is needed, which suggests that the particulate outflow boundary could have a slightly large opening to increase the mass outflow.

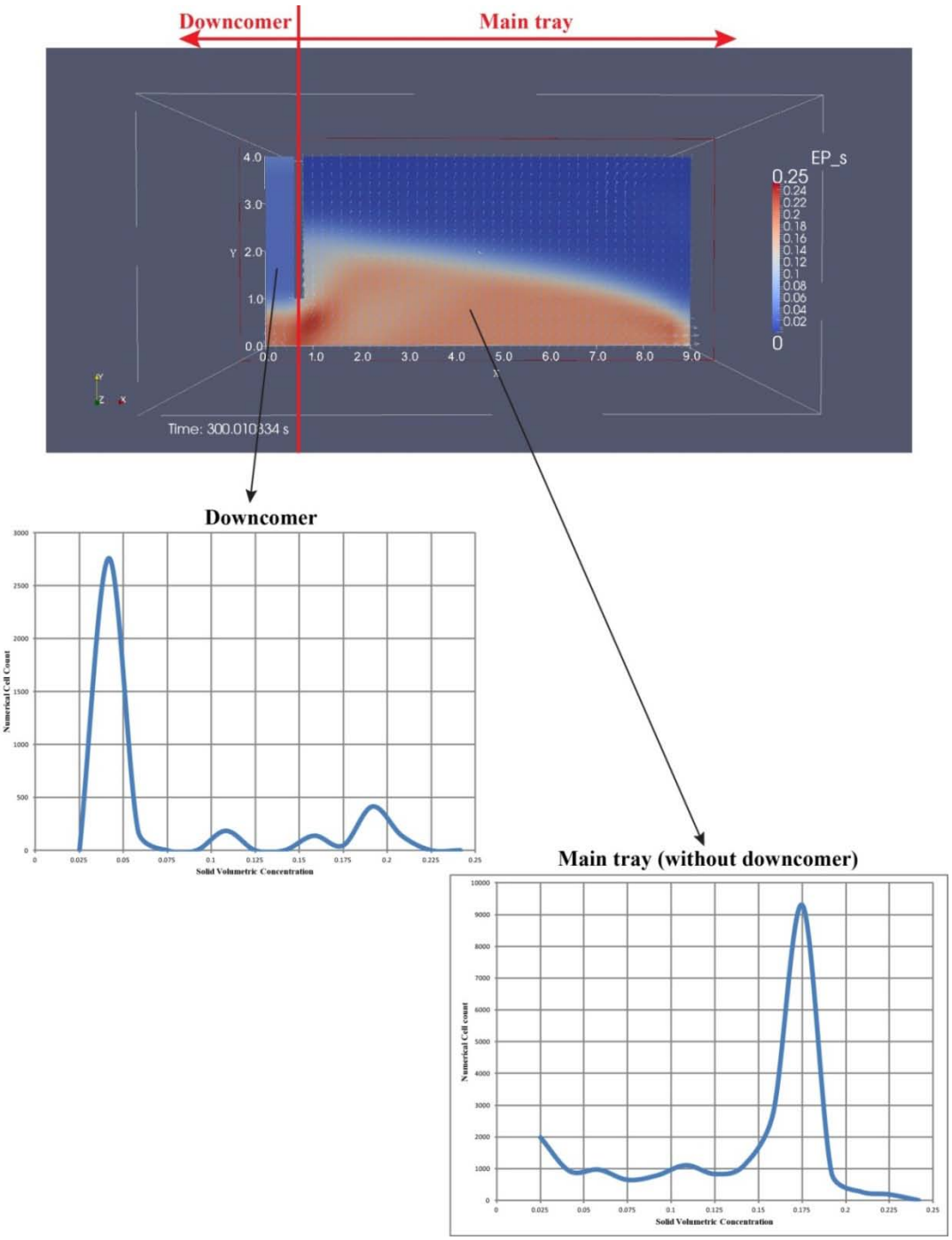

Figure 2.9. Histogram distribution of the solid volumetric concentration in the downcomer (left) and the rest of the tray (right) at 300 s. This explains the bimodal distribution in Figure 2.8. The dilute mode is due to the particles flowing down from the top inlet in the downcomer. This indicates that at steady state, the main mode is at 0.175.

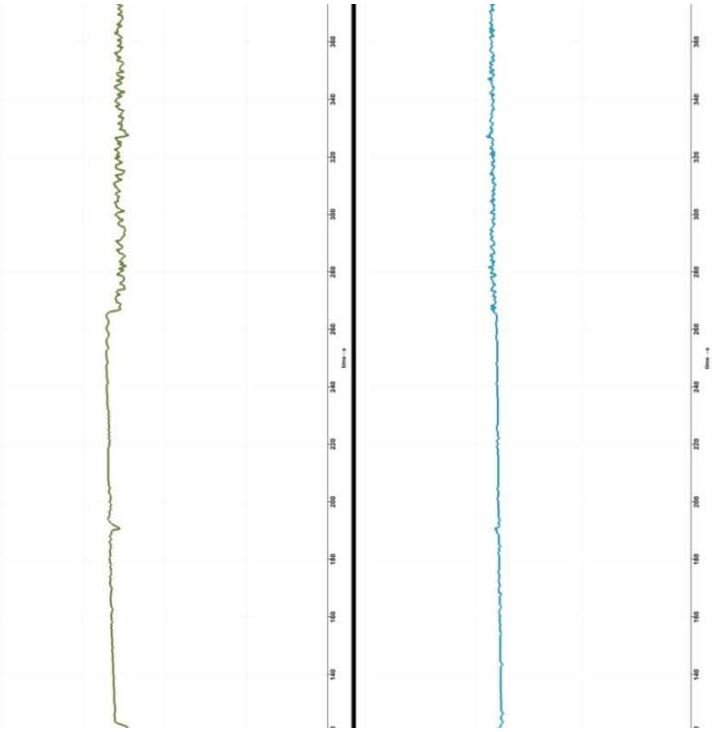

Figure 2.10. Solid volumetric concentration (ε_s) top and magnitude of the solid (m/s) at the outlet of the tray (bottom right-hand side). Note: after 30 s, a steady state is reached at the outlet.

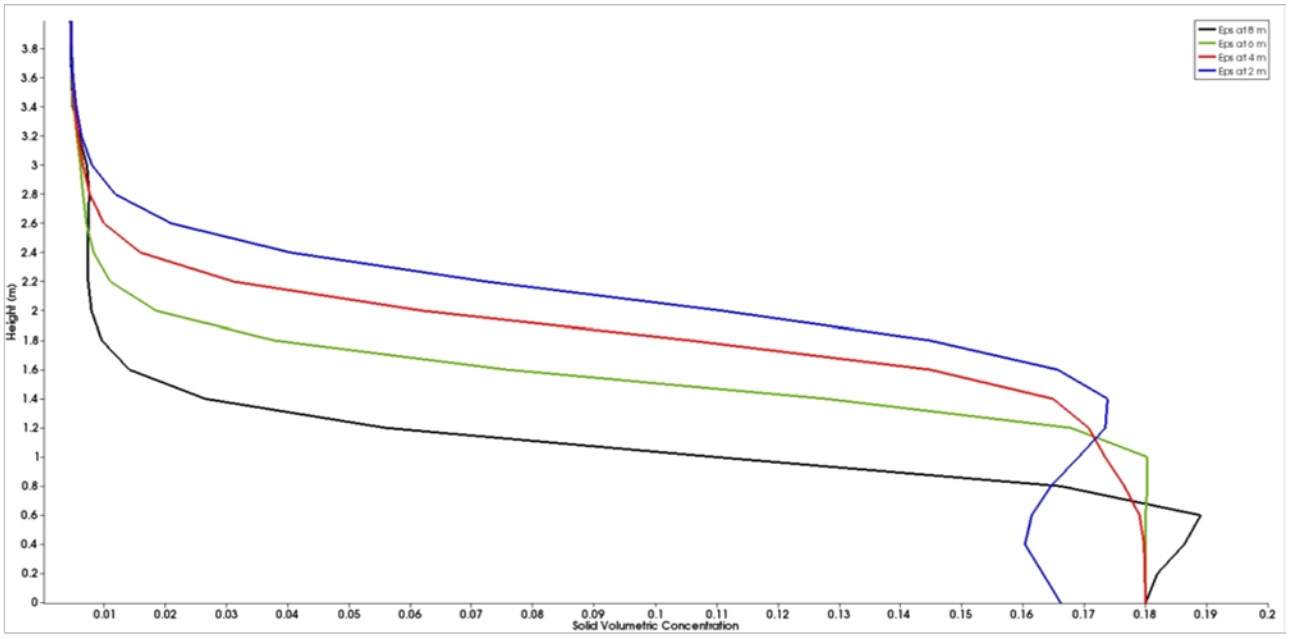

Figure 2.11. Solid volumetric concentration versus height at 300 s and at four different positions within the tray. The nearer to the outflow exit, the lower the height of the fluidized bed as shown by the black curve (the blue curve is 2 m away from the downcomer).

Caption for Figure 2.12 (35 kg/s, page 18). Solid volumetric concentration (blue = no solid; red= more solid) taken at different time. The glyph represents the velocity vector of the gas phase (note the particle clustering and heterogeneous volumetric distribution throughout the tray).

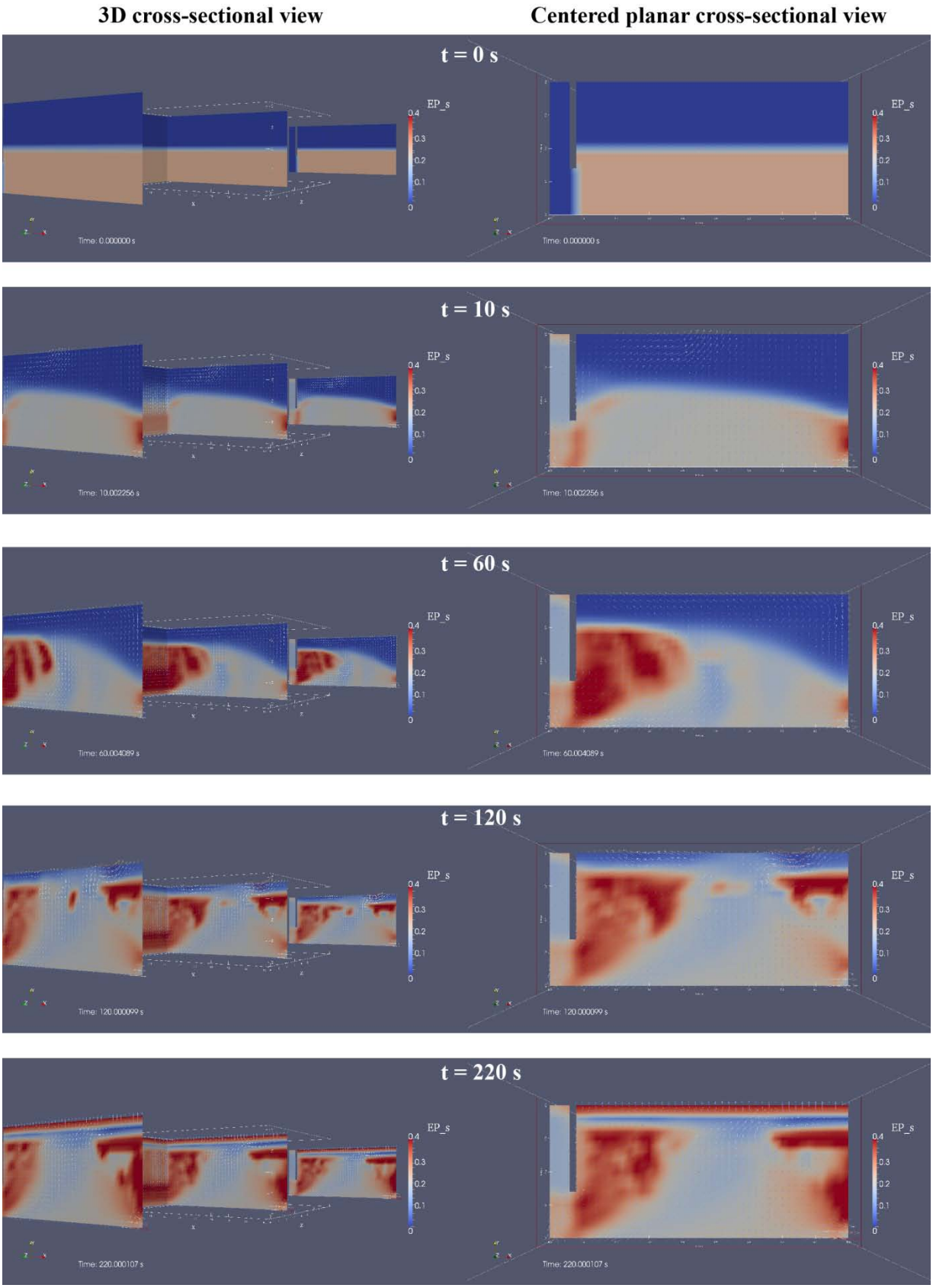
3D cross-sectional view
Centered planar cross-sectional view
t = 0 s
t = 10 s
t = 60 s
t = 120 s
t = 220 s
EP_s
0.4
0.3
0.2
0.1
0
Time: 0.000000 s
Time: 10.002256 s
Time: 60.004089 s
Time: 120.000099 s
Time: 220.000107 s

Figure 2.12.

2.4.3. Other simulations

Other simulations have been performed to explore the free parameter space in terms of particulate down influx and geometry configuration of the wall between the downcomer and the rest of the tray. One issue was to increase the height of the fluidized bed and/or increase the particulate content in the tray. One would have wanted to increase the bed height to 3 m (the last top meter without the cooling rods would be a particle-free board) and/or the particulate content up to ε_s ~0.2-0.3 without the undesirable clustering effects.

For example, Figure 2.13 shows one of these "exploratory" simulations in which all is identical from the previous simulation 40 kg/s except the influxes at the boundaries and the initial granular bed porosity:

Initial granular bed porosity, ε_s =	0.25
Vertical speed of flue gas at bottom inlet, $V_{g,y}$ =	0.345 m/s (or 35 kg/s mass flux)
Vertical speed of solid sorbents at top inlet, $V_{s,y}$ =	-0.20 m/s (or 120 kg/s mass flux)

The very large mass influx of particles creates an especially chaotic dynamical system that is unable to reach a steady state and creates an important solid cluster (as shown in the multimodal distributions of Fig. 2.13).

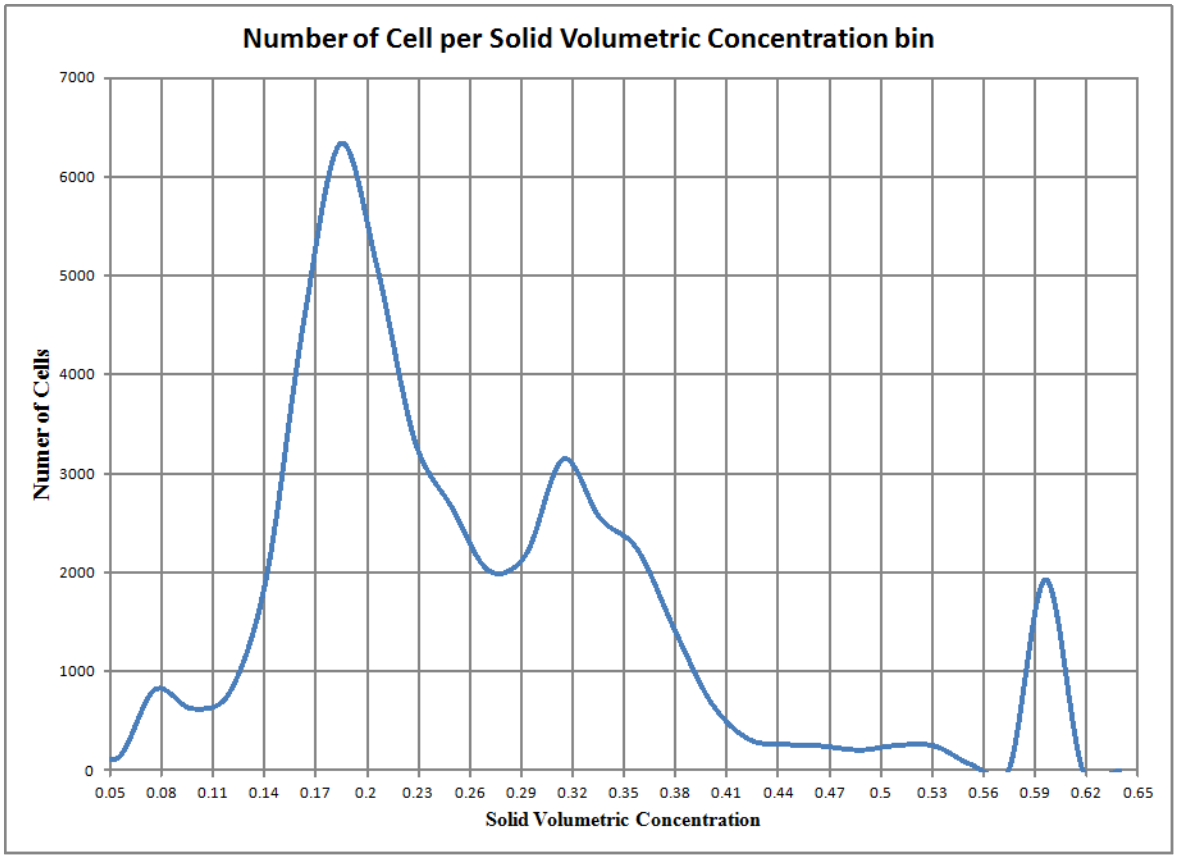

Figure 2.13. Histogram distribution of the solid volumetric concentration in the whole tray domain at 220 s (see Fig. 2.12). Note the solid volumetric concentration multi-modes, particularly the peak at 0.61, which represent a solid cluster.

2.5. Summary of adsorber results

Parametric investigations to study the influence of operating conditions were performed. The flue gas and particle inlet velocity were found to have the largest impact on flow dynamics of sorbent and gas in the adsorber trayed column. We found that the ideal performance for the adsorber would be assessed by well-homogenized fluidization (i.e., without particle clusters), by enough particle mean residence time ~$O_{(10\ min)}$, an optimal bed height (~3 m), and enough particles available for the adsorption processes in this system (~20-30 vol.%). However, these conditions are not fully compatible with each other. We determined the best compromising results were achieved with a flue gas fluidization up speed of ~64·U_{mf}, achieving a particulate mean residence time of ~40 minutes. However, this flow still is fairly dilute (~17 vol.%) and only reaches a nominal height of 2 m. Potentially, better results could be achieved in incrementally increasing the downward solid mass fluxes. Another possibility, as explored for the regenerator, is to increase the size of the solid sorbent particles. Clearly, this CFD analysis has shown that the flue gas mass influx, as initially set by Task-3, ~100·U_{mf}, was unreasonably high.

To determine the best combinations of boundaries (inlets/outlets), mass fluxes, initial conditions for generating the optimal fluidized circulating granular bed, we propose to continue iterative, different multiphase 3D simulations within the single-stage granular bed. Then, we will rerun the simulation over a two-staged granular bed (a whole adsorption column). At a later stage, we propose to incorporate chemistry models.

3. Modeling the Regenerator

This report presents a CFD model for the flow of solid particles and steam in the regenerator. The goal is to demonstrate the modeling capabilities using multiphase flow simulations. The information obtained from these simulations will be useful to optimize the design of the full-scale regenerator, determine the most efficient operating conditions, and eventually predict the regenerator's performance efficiency *in silico*. Parametric studies are performed for varying operating conditions (steam inlet velocity, solids holdup, and solids inlet flow rate), regenerator design (plate spacing), and sorbent properties (particle size).

The present work focused on the flow dynamics of sorbent particles and gas in the regenerator. The chemical reaction involved in regenerating fresh sorbent particles is not included. Understanding the influence of operating and design conditions will assist in achieving the desired flow conditions in the regenerator. The amount of CO_2 regeneration is expected to be strongly correlated to the mean residence time of sorbents, i.e., particles that remain longer are more likely to be fully regenerated.

3.1. Modeling approach

3.1.1. The multiphase flow model

The multiphase flow inside the regenerator consists of the sorbent particulate phase, CO_2 released from the sorbent as gas, superheated steam injected to fluidize the particles and to promote CO_2 release, and some ambient air. In addition, the A50.1 design also has stationary perforated porous plates horizontally placed within the regenerator. The purpose of these plates is to improve and regulate residence time of sorbent particles in the regenerator. To simplify the problem, only steam is currently considered in the gas phase because reaction kinetics is not yet included in the present model. This is a reasonable simplification as both superheated steam and CO_2 behave as Newtonian fluids with similar viscosities and density values compared to the solid phase. Moreover, the flow dynamics in the regenerator is dominated

by the solid phase. It is expected that excluding CO_2 from the multiphase model will not change the results qualitatively.

The multiphase flow model (Gidaspow 1993) is formulated based on conservation of mass, momentum, and energy for each individual phase in the flow. Additional constitutive equations are used to close all conservation equations and couple different phases. For example, the gas phase is considered to be a Newtonian fluid, whereas the interaction between the gas and flowing sorbent particles are modeled using the Wen-Yu drag correlation (Wen and Yu 1966). Details regarding the flow models can be found in Gidaspow (1993). The governing equations are solved numerically using MFIX developed by NETL, which is a well-established, open-source code used to model a range of multiphase flows.

For the present simulations, the flow is assumed to be isothermal, and energy conservation equations are not considered. In the actual regenerator, the temperature is expected to vary between 120-150°C, a range wherein gas properties do not change significantly.

3.1.2. Regenerator design and model geometry

A schematic of the regenerator provided by Task-3 is shown in Figure 3.1. Depleted sorbent particles exiting the adsorber enter the regenerator from the top and travel downwards under the action of gravity. A series of perforated horizontal plates help evenly distribute the weight of the solids and promote heat transfer to the particles. Superheated steam, which aids the release of CO_2 by the sorbents, is injected into the device from the bottom and flows upward through the perforated plates and solids. The regenerated sorbent particles leave the particle from the bottom of the regenerator before being fed back again to the adsorber. The superheated steam, rich with the CO_2 released by the sorbents, leaves the regenerator from the top for separation and sequestration.

The target of the full-scale CCSI regenerator is to process approximately 500-600 tons of sorbent per hour. To handle such flow rates, the characteristic dimension of the regenerator is on the order of 10 m × 10 m × 10 m. The regenerator's efficiency, determined by the degree of regeneration of the sorbent particles, is strongly influenced by the residence time of the solids in the regenerator. It is expected that a longer residence time will promote better regeneration of the sorbents. The amount of residence time needed for adequate regeneration depends on the sorbent particles' chemical and physical properties. For the present work, a residence time of 10 minutes is expected to suffice and is the target for this device.

The perforated plates consist of relatively thin plates (compared to system height) with an array of regularly spaced holes. Some of the plate parameters include spacing between the holes, the hole's size, and spacing between plate layers. The characteristics of the plate may influence the residence time distribution of the sorbent but not the mean residence time. It should be noted that mean residence time depends only on the inlet flow rate and steady state solids holdup and is independent of the internal structures or flow inside the regenerator. In this work, except for the plate layer spacing (to be discussed later), the plate characteristics were not investigated.

The size of the regenerator in the proposed design is 10 m × 10 m × 10 m. Because the full 3D system is too expensive for available computational resources, a two dimensional (2D) model is simulated instead. It is expected that predictions from a 2D system may differ quantitatively from the 3D system but will not affect the results qualitatively. Furthermore, because simulating the entire 10 m width is not advisable when performing parametric studies, a sliced 2-m-wide column of the full domain extent is used. A schematic of the geometry simulated using MFIX is shown in Figure 2.2. The next section shows that boundary conditions on the sides of the 2-m-wide column do not affect the sorbent or gas' overall flow behavior.

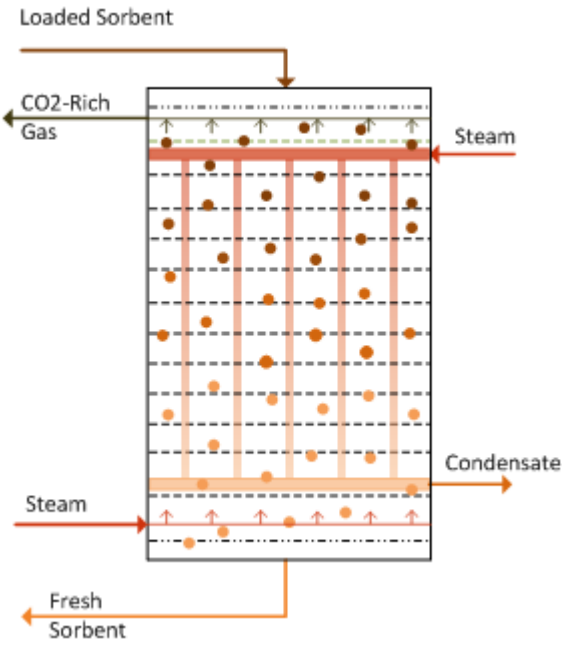

Figure 3.1. (*Above*) Schematic of the CCSI regenerator devised by Task-3. Solid particles flow downward from the top inlet to the outlet at the bottom through a series of perforated plates. Superheated steam enters at the bottom and exits from the top outlets.

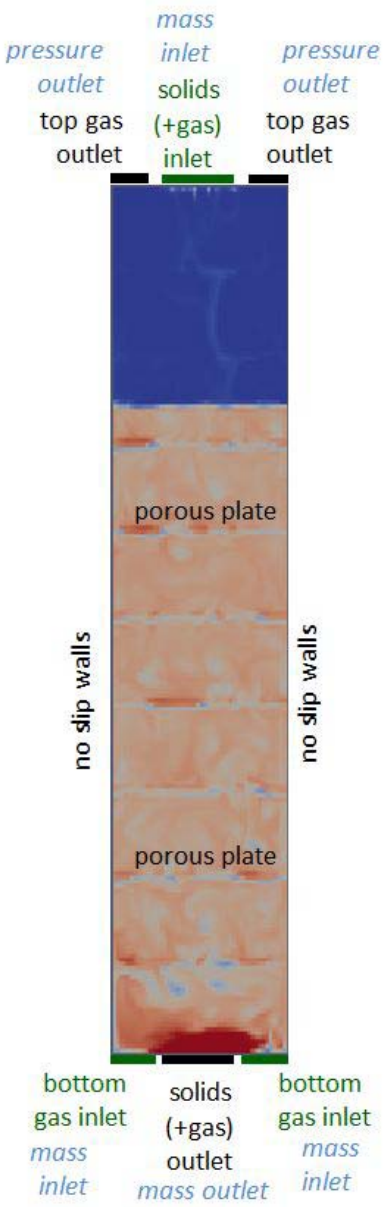

Figure 3.2. (*Right*) Simplified model of the regenerator using MFIX. The perforated plates are modeled as a series of stationary, uniformly porous layers. Instead of the full 3D system, a single 2D column 10-m tall and 2-m wide is simulated.

The boundary conditions used for the system are shown in Figure 3.2. The solids inlet is modeled as a mass inlet in the middle of the top of the regenerator column. The solids flow rate is specified to be 3 kg/s through the sorbent inlet of area 2 m^2 at the top, which corresponds to 540 ton/h for the full-scale 10 m × 10 m cross section. The gas (modeled as steam) that occupies the interstices between the entering solid particles is assigned an inlet velocity comparable to the solids inlet velocity. The corresponding solids outlet at the bottom of the regenerator is specified as a mass outlet in MFIX with the solids and gas outflow rate set equal to the inlet flow rate at the top. As the solids flow rate at the top inlet and bottom outlet are set to be the same, the steady state mass holdup in the regenerator does not change. Note that the mass holdup may also be expressed as the bed voidage, which is the volume fraction occupied by the

gas and is computed by subtracting the solids holdup volume fraction from unity. This steady state sorbent holdup can be specified through the initial conditions and is a controllable parameter for the simulations.

The mass inlets for superheated steam are situated at the bottom of the regenerator column on either side of the solids outlet. The inlet mass flow rate for steam is a controllable parameter and one of the parametric investigations in this work. The gas outlets are positioned at the top of the column on both sides of the solids inlet. The gas outlets are modeled as pressure outlets in MFIX. To prevent sorbents from flowing out, the gas outlets are surrounded by semi-permeable membranes that allow only gases to pass through.

To accurately model the flow of gases and sorbents around the plate perforations, mesh size would have to be much smaller than the hole size, i.e., *O*(1 mm). Because using such a fine mesh is infeasible for the simulation of a 10-m-tall device, an alternate strategy for simulating the plates is developed, where a uniform porous media is used to represent the perforate plates. Such a porous media would provide the necessary resistance to the flow of solids and gas passing through the plates, effectively simulating the behavior of the real plates. Because the flow of solids in the regenerator is more important than the flow of gas, the drag resistance provided by the porous media needs to be matched with the resistance from the real plates. The drag force, F_{12}, between the stationary plate phase and the flowing sorbent phase is given by (Syamlal 1987; Gera et al. 2004) as:

$$F_{12} = \frac{3\left(1+\varepsilon_{12}\right)\left(\frac{\pi}{2}+\mu_{12}\frac{\pi^2}{8}\right)\phi_1\rho_1\phi_2\rho_2\left(d_1+d_2\right)^2 g_{0,12}\left|\vec{v}_1-\vec{v}_2\right|}{2\pi\left(\rho_1 d_1^3+\rho_2 d_2^3\right)}, \tag{3.1}$$

$$g_{0,12} = \frac{1}{\phi_g}+\frac{3d_1d_2}{\phi_g^2\left(d_1+d_2\right)}\left(\frac{\phi_1}{d_1}+\frac{\phi_2}{d_2}\right), \tag{3.2}$$

where the subscripts "*1*" and "*2*" refer to the two solid particulate phases and "*g*" refers to the gas phase. The symbols ε_{12}, μ_{12}, and $g_{0,12}$ represent the normal restitution coefficient, friction coefficient, and radial distribution function for the two solid phases. The volume fractions, densities, particle diameters, and velocities of both phases are denoted by ϕ, ρ, d, and $\vec{v}$, respectively. Equations (3.1)-(3.2) show that a number of parameters for the porous media phase need to be mapped to real plate parameters to simulate flow through plates accurately. A systematic study for mapping these parameters is beyond the scope of the current work. Presently, constant baseline values of ϕ_1 = 0.1 and d_1 = 2 mm are used, where subscript "*1*" refers to the porous plate solid phase. Some preliminary efforts to map the plate properties to the porous media parameters are discussed in the Appendix of this report.

To obtain accurate numerical solutions, high enough resolution is necessary. In the present work, 200 total cells are used along the vertical (Y) direction, and 48 cells are used along the horizontal (X) axis. Using a smaller mesh size is expected to resolve the finer features of the flow but is impractical for parametric studies. Moreover, further increasing the resolution is not expected to significantly affect flow predictions. This hypothesis will be verified in the next portion of our work. All simulations are performed at isobaric (1 atm = $1.01\text{x}10^5$ Pa) and isothermal (383 K = 110°C) conditions.

3.1.3. Setup of boundary conditions

As the modeled column represents a portion of the full regenerator, symmetric conditions, such as periodic or free-slip walls, are more suited for the side boundary conditions. To investigate the choice of boundary conditions, results are compared for free-slip side walls, periodic sides, and even no-slip side walls. A representative case of 150 µm particle diameter, ~30% solids volume fraction, solids flow rate of 3 kg/s, and inlet steam velocity of $5U_{mf}$ (= 5 × 0.00852 m/s) is used for this study.

From snapshots of three different boundary conditions in Figure 3.3, the steady state solids distribution after 200 s appears to be almost the same. Small differences in local densities can be attributed to the continuous formation and dissipation of particle clusters. Animations of the three cases do not reveal any noticeable differences in the formation or spatial distribution of these particle clusters.

To quantitatively compare the influence of the side boundary conditions, the distribution of sorbent volume fraction along the regenerator height is shown in Figure 3.4. The distribution at 200 s reveals that the influence of the side boundary conditions is insignificant and any differences are within the range of fluctuations associated with clustering behavior. As the data presented in Figure 3.4 averages over all locations along the horizontal direction, the frequency distribution of solids volume fraction in all of the cells is presented in Figure 3.5.

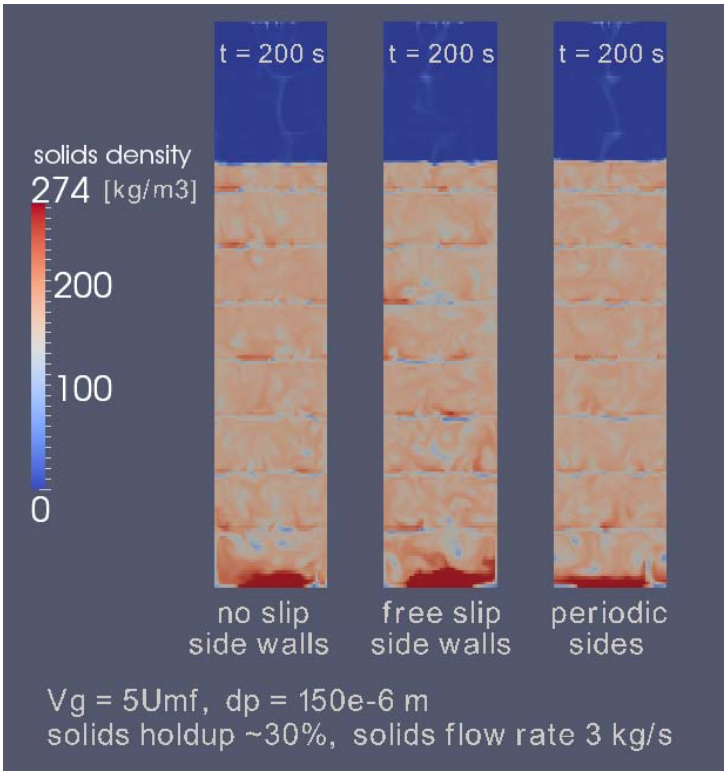

Figure 3.3. Comparison of solids density distribution for three different boundary conditions: no-slip side walls, free-slip side walls, and periodic sides. Snapshots at 200 s do not reveal any qualitative differences in the solids distribution. Simulations performed for baseline conditions of 150 µm particle diameter, ~30% solids holdup, 3 kg/s solids flow rate, and steam inlet velocity of $5U_{mf}$ (= 5 × 0.00852 m/s).

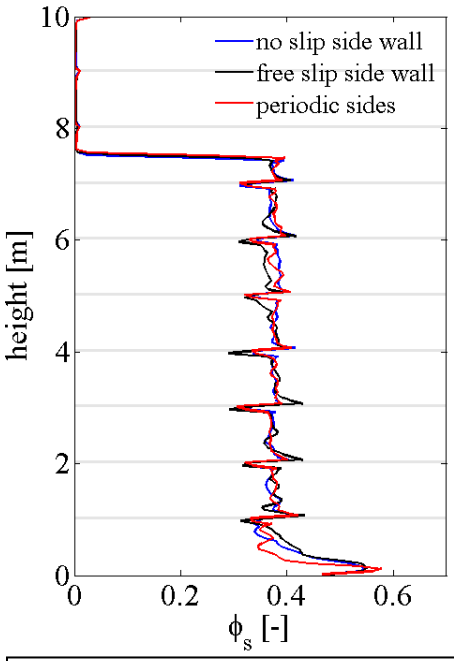

Figure 3.4. Distribution of solid volume fraction along height for the three different side boundary conditions. The boundary conditions do not affect the profile, and the differences are within the variations associated with clustering instabilities.

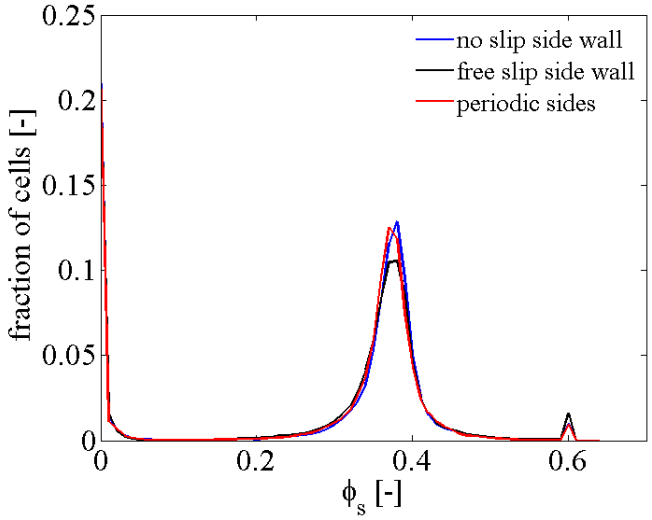

Figure 3.5. Frequency distribution of solid fraction in all of the cells. The first mode represents the empty blue regions (Fig. 2.3); second mode, the particle rich bed; and third mode, the packed red regions above the outlet. The choice of boundary conditions does not affect the frequency distribution.

Frequency distributions are obtained by recording the solids volume fraction in each cell over 10 s, capturing any clustering behavior within this time interval. Three modes for the solids fraction distribution are observed. The first mode at $\phi_s \sim 0$ represents the empty space above the particle bed (blue regions in Fig. 3.3). The second mode represents the bulk of the particle bed where particles have an intermediate density of less than 0.4. A mode at $\phi_s \sim 0.6$, reflecting the small packed region immediately above the outlet, is also shown.

A comparison of the three boundary conditions establishes that the choice of side boundary conditions do not affect the flow predictions, even for the no-slip wall case. For the remainder of this study, the side walls are modeled as no-slip walls as there is almost no qualitative or quantitative differences between the three boundary conditions examined.

3.1.4. Verification of steady state flow

After an initial startup period, the multiphase flow in the regenerator reaches a steady state. To examine if a flow has reached its steady state in a simulation, some transient results should be compared at different times. Here, the particle volume fraction distribution along the height of regenerator is compared at three different times. As shown in Figure 3.6, the obtained profiles for 150 s, 180 s, and 200 s overlap each

other. Therefore, the flow is determined to have reached its steady state after 150 s. The results taken at 200 s were used to perform our steady state measurements.

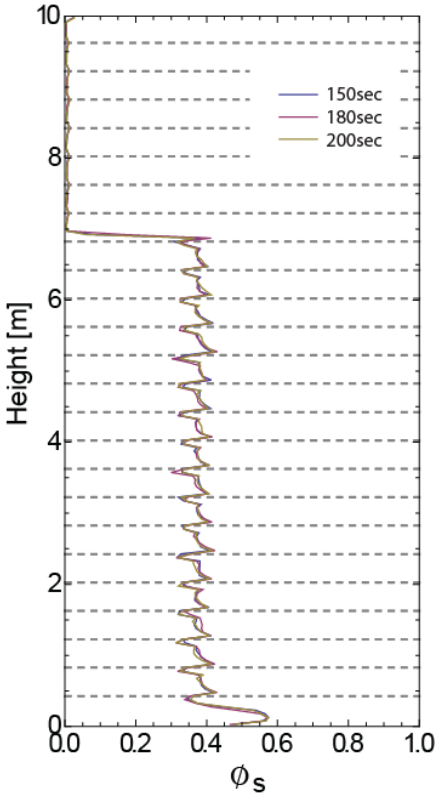

Figure 3.6. Distribution of solid volume fraction along height at the three different times. The stationary porous plates placed in the regenerator are marked by dashed lines.

3.2. Results

3.2.1. Typical flow behavior inside the regenerator

The regenerator consists of two concurrent streams: particles flowing downward under gravity and superheated steam rising upward through the particles and plates under pressure gradient. The mean residence time $\bar{t}_{res}$ of the particles is given by:

$$\bar{t}_{res} = \frac{m_{holdup}}{Q}, \tag{3.3}$$

where m_{holdup} is the steady state mass holdup and Q is the mass flow rate. In these simulations, the mass flow rate is specified by the target flow rate, and the holdup solids mass can be controlled by adjusting the inlet and outlet conditions in an actual regenerator. For a prescribed flow rate of 3 kg/s and a target mean residence time of at least 10 minutes, a solid volume fraction value of $\phi_s \sim 0.3$ is a suitable choice.

For the given solid flow rate and regenerator dimensions, the superficial velocity of solids is *O*(0.01 m/s), which is smaller than the superficial velocity of gases expected within the regenerator. As such, the flow and clustering behavior of particles is dominated by the upward flowing gas. Figure 3.7 shows the typical velocity vectors for gas and solids superimposed on the solids density contours. The plate properties chosen for these studies are such that the maximum possible flow rate through each plate is larger than the

inlet/outlet flow rate. This ensures that particles are able to flow downward through the plates faster than the inlet flow and accumulate in the lower regions instead of jamming at the top.

The superficial velocity of inlet steam is chosen so it does not form a spouted particle bed. Particles entering the regenerator initially fall through the mostly empty region at the top and gradually move downward under gravity through the more dense lower regions. In the presence of the fluidized bubbling bed, an interface between the dense lower regions and sparse top region often can be identified. In Figure 3.7, particle velocities are found to follow the gas velocities quite closely. This is mostly due to entrainment of solids in the faster flowing gas, especially if the particles are smaller and lighter. Both particles and gas have larger velocities in the less dense top regions. In the lower regions with larger solids density, energy is rapidly dissipated through inelastic particle collisions, which results in smaller velocity magnitudes.

The exact variation of solids density, residence time distribution, and flow patterns depends on the choice of regenerator design, operating conditions, and particle properties. The following sections examine the influence of gas inlet velocity, solids holdup, spacing between plates, and particle size on flow dynamics in the regenerator.

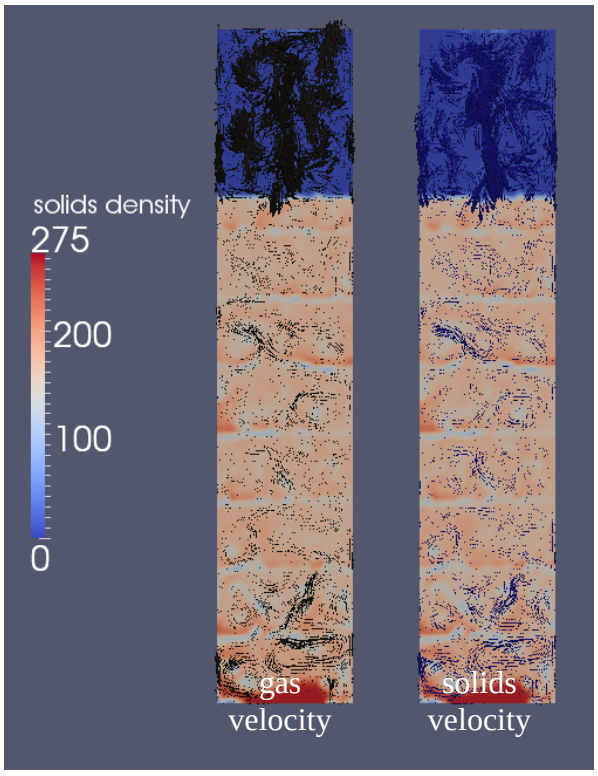

Figure 3.7. Velocity vectors for gas flow (left) and particle flow (right) overlaid on the solids density. Particles get entrained with the faster moving gas, especially for smaller and lighter sorbents, and follow the gas velocities. Velocities are smaller in the lower regions with larger solid packing fractions.

3.2.2. Effect of varying steam inlet velocity

For gas-particle multiphase flows, an important quantity is the minimum fluidization velocity. The minimum fluidization velocity, U_{mf}, is the upward superficial velocity of the gas when the weight of the particle bed is exactly balanced by the drag exerted by the gas on the particles. If the superficial gas

velocity is increased beyond U_{mf}, the bed starts to fluidize. The minimum fluidization velocity is given by (Geldart 1973):

$$U_{mf} = \frac{\left(\rho_s - \rho_g\right) g d_p^2}{150\mu_g} \cdot \frac{\phi_{s,mf}^3}{\left(1-\phi_{s,mf}\right)}, \tag{3.4}$$

where ρ_s and ρ_g are the solids and gas densities, d_p is the particle diameter, and μ_g is the gas viscosity. The solids volume fraction at the point of minimum fluidization is denoted by $\phi_{s,mf}$ and typically lies between 0.40-0.45. Fluidized beds are typically operated at $30U_{mf}$, sometimes going up to $100U_{mf}$. For the regenerator, fluidization of the particles should be avoided and gas velocities limited to less than $30U_{mf}$. The value of U_{mf} for the 150-µm sorbent particles is computed to be 0.00852 m/s at $\phi_{s,mf}$ = 0.45. In this section, the effect of inlet gas (steam) superficial velocity, $V_{g,sup}$, is investigated.

As the inlet gas velocity is increased, the bed of solids at the bottom experiences greater fluidization. The density of solids in the lower regions decreases with a corresponding increase in the height of the free surface (Figure 3.8 and Figure 3.9). At larger inlet velocities $V_{g,sup} > 10U_{mf}$, material tends to accumulate at the top of the regenerator as a packed bed. For an even larger inlet velocity of $20U_{mf}$, a large fraction of particles eventually migrate to the top and form a densely packed bed (rightmost column in Fig. 3.8), a condition detrimental to the device's performance which should be avoided. Figure 3.9 shows the variation of solids density does not change with height except in the vicinity of the outlet region. The minimum fluidization velocity calculated by Equation 3.4 provides a physical estimate for the maximum permissible inlet gas velocity for any choice of sorbent material and properties. To avoid a packed bed of material at the top of the regenerator, the inlet gas velocity is fixed at five times U_{mf} for the remaining parametric studies presented for the regenerator.

As the mean residence time is dependent only on the solids holdup and mass flow rate, the mean residence time is calculated as:

$$\bar{t}_{res} = \frac{m_{holdup}}{Q} = \frac{\rho_s \phi_{s,avg} \left(A_{CS} h\right)}{Q} = \frac{441 \text{ kg/m}^3 \times 0.2854 \times \left(20 \text{ m}^3\right)}{3 \text{ kg/s}} = 839 \text{ s} \approx 14 \text{ min}, \tag{3.5}$$

where $\phi_{s,avg}$ is the average solids volume fraction and $\left(A_{CS} h\right)$ is the volume of the regenerator modeled. The mean residence time for all inlet steam velocity conditions is the same because the holdup mass and flow rate are not varied. The achieved mean residence time of 14 minutes is larger than the target residence time of 10 minutes and is expected to result in regenerated particles that are almost fully regenerated.

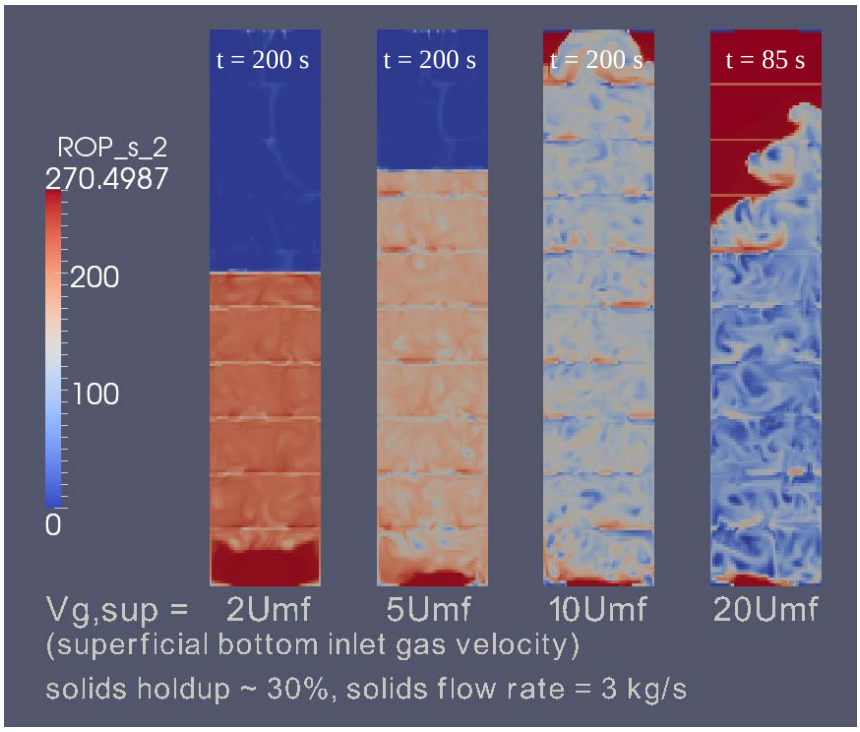

Figure 3.8. (*Top*) Solid fraction distribution for varying steam inlet superficial velocity, $V_{g,sup}$, expressed as a multiple of the minimum fluidization velocity, U_{mf}. The density of solids decreases at larger inlet steam velocities. At $V_{g,sup}$, values larger than $10U_{mf}$, sorbent particles migrate to the top and accumulate as a packed bed, which is detrimental to device performance.

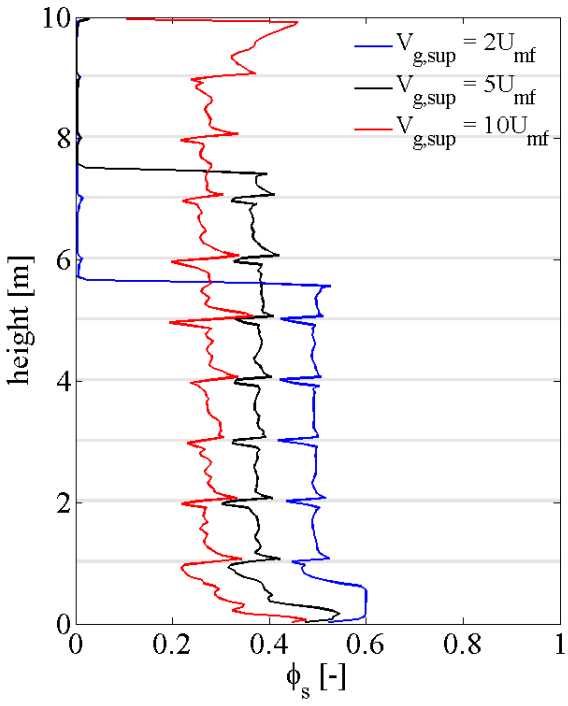

Figure 3.9. (*Right*) Average solid fraction distribution in horizontal layers as a function of height at 200 s. The steady state solid fraction decreases with increasing inlet steam velocity along with a rise in the height of the free surface interface. At $V_{g,sup}$, larger than $10U_{mf}$, sorbents are found to accumulate at the top of the device.

3.2.3. Effect of varying solids holdup

The mean residence time for a given flow rate can be controlled through the solids holdup. The influence of varying holdup (thus changing the residence time) on solids distribution must be investigated to identify any potential changes in flow behavior.

Figure 3.10 illustrates that the solids holdup does not affect the distribution of solids density in the lower regions of the regenerator. An increase in the holdup results in a higher location for the free surface interface. At holdup fractions of 40% and greater by volume, material is shown to accumulate as a packed bed at the top of the regenerator. The case of approximately 50% holdup by volume (not shown in Fig. 3.10), packing behavior similar to the $20U_{mf}$ case in Figure 3.8, was observed. As a packed bed at the top of the regenerator is undesirable, the solids holdup should be maintained below 40% by volume for a gas inlet velocity of $5U_{mf}$. This maximum permissible value for solids volume fraction would increase at smaller gas inlet velocities and decrease for larger inlet velocities.

As the solids holdup varies while maintaining a constant mass flow rate (3 kg/s), the mean residence time of sorbents also is affected. Table 3.1 lists the mean residence time for varying solids holdup calculated using Equation (3.5).

Table 3.1 Mean Residence Time for Varying Solids Holdup for 3 kg/s Inlet Solids Flow Rate

	20% holdup	**30% holdup**	**40% holdup**	**50% holdup**
Mean residence time	588 s, or 9.8 min	882 s, or 14.7 min	1176 s, or 19.6 min	1470 s, or 24.5 min

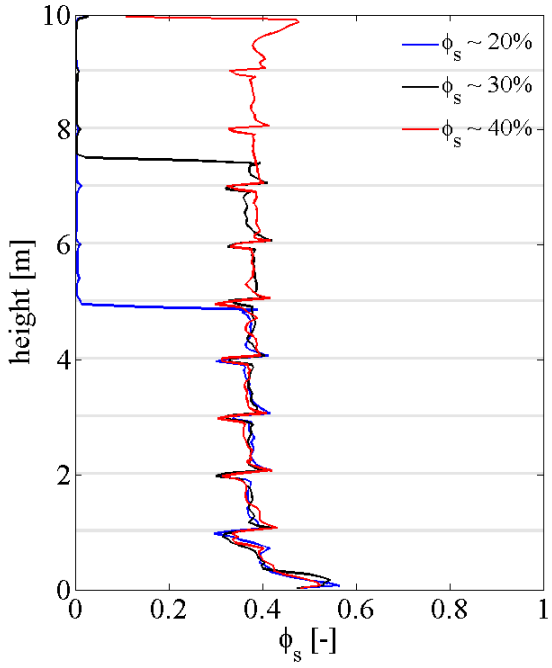

Figure 3.10. Distribution of solid fraction along height for varying steady state mass holdup. Increasing the holdup does not affect the density or distribution of particles in the lower regions but increases the free surface height. Beyond 40% holdup by volume, material is shown to accumulate at the top as a packed bed (similar to Fig. 3.8, $20U_{mf}$ case).

3.2.4. Effect of varying solids flow rate

The desorption of CO_2 from depleted sorbent particles can be linked to the solids residence time in the regenerator—a longer residence time more likely produces better-quality regenerated sorbents. The exact length of time required for adequate regeneration (e.g., determined by 90% or 99% desorption) depends on the sorbent used. At present, the residence time required is not determined exactly but is estimated to be approximately 10 minutes. If a mean residence time shorter than 10 minutes is sufficient, a smaller regenerator cross section may be able to handle the prescribed flow rate, thereby increasing the mass flow per unit area. The influence of increasing the mass flow rate, i.e., the flow rate in the present 2 m × 1 m column, on flow and solids distribution is presented.

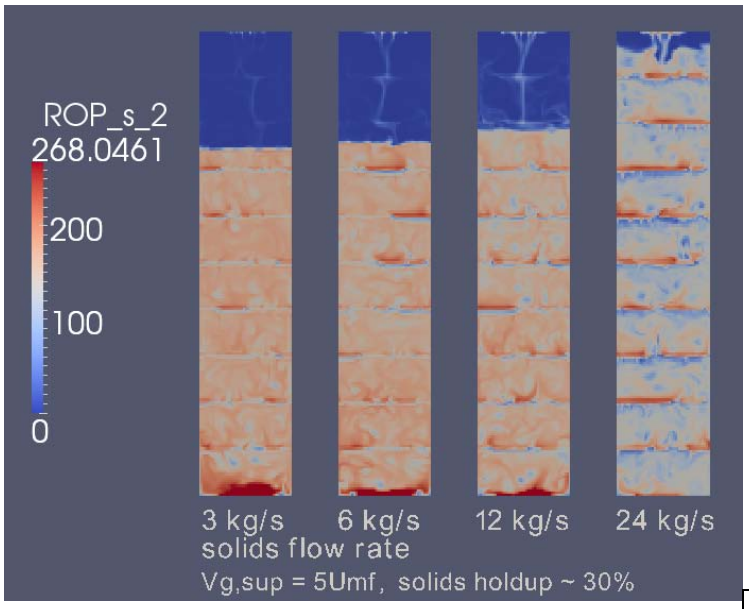

Figure 3.11. Solid fraction distribution contours at 200 s for varying inlet mass flow rate. No significant changes in solids holdup are observed up to 12 kg/s, beyond which solids are distributed more evenly in every stage. The mean residence time decreases as the inlet flow rate is increased.

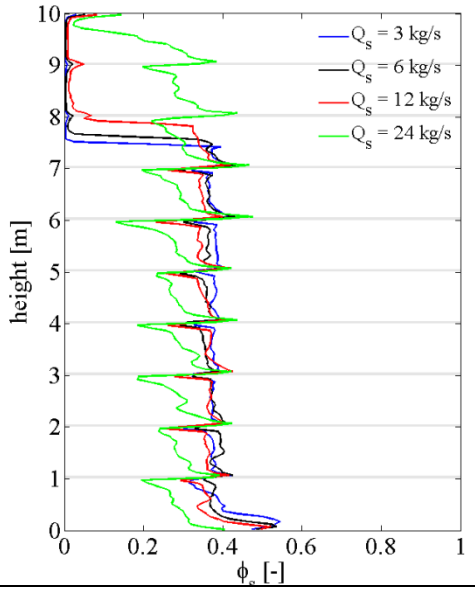

Figure 3.12. Solid fraction distribution along height for varied inlet mass flow rates. The 3 kg/s, 6 kg/s, and 12 kg/s have similar distribution of solids. Particles occupy the topmost sections at larger flow rates. Note the total solids holdup is the same (28.5%) for all cases.

Increasing the solids flow rate from 3 kg/s (over the modeled area of 2 m^2) up to 12 kg/s does not have a significant effect on the solid fraction distribution (Fig. 3.11 and Fig. 3. 12). At a much larger flow rate of 24 kg/s, solid particles are found to reside even in the topmost sections. This difference in behavior can be qualitatively explained by considering two time scales: 1) the time scale associated with the inlet flow rate and 2) the time taken by particles to pass through a plate. If the time taken for particles to pass through a plate is much shorter compared to the rate of entry for new particles, most of the particles will quickly fall and form a bed in the lower part of the regenerator. This phenomenon occurs at 3 kg/s, 6 kg/s, and 12 kg/s. If the two time scales are comparable, particles enter the system at a rate comparable to the rate at which they pass through the plates, ensuring particles leaving a region are replenished simultaneously. This results in a more uniformly filled device with little empty space, such as the 24 kg/s case. Note the mean residence time is inversely proportional to the solids inlet flow rate (Eq. (3.5)). The mean residence time for the four cases presented in Figures 3.11 and 3.12 are listed in Table 3.2. The maximum flow rate

(per unit area) while maintaining a sufficiently long residence time can be determined using Table 3.2 and Equation (3.5).

Table 3.2 Mean Residence Time for Varying Inlet Solids Flow Rate at Constant Holdup of 28.5% by Volume

	3 kg/s	**6 kg/s**	**12 kg/s**	**24 kg/s**
Mean residence time	838 s, or 14.0 min	419 s, or 7.0 min	209 s, or 3.5 min	105 s, or 1.7 min

3.2.5. Effect of vertical spacing between perforated plates

The perforated plates are introduced in the regenerator to enhance recycling efficiency of depleted sorbent particles. Thus, the number of plates and spacing between them are important design parameters. In this section, three different design conditions—9 layers (1.0 m apart), 24 layers (0.4 m apart), and 49 layers (0.2 m apart)—are considered for simulating gas and particle flow in a reactor.

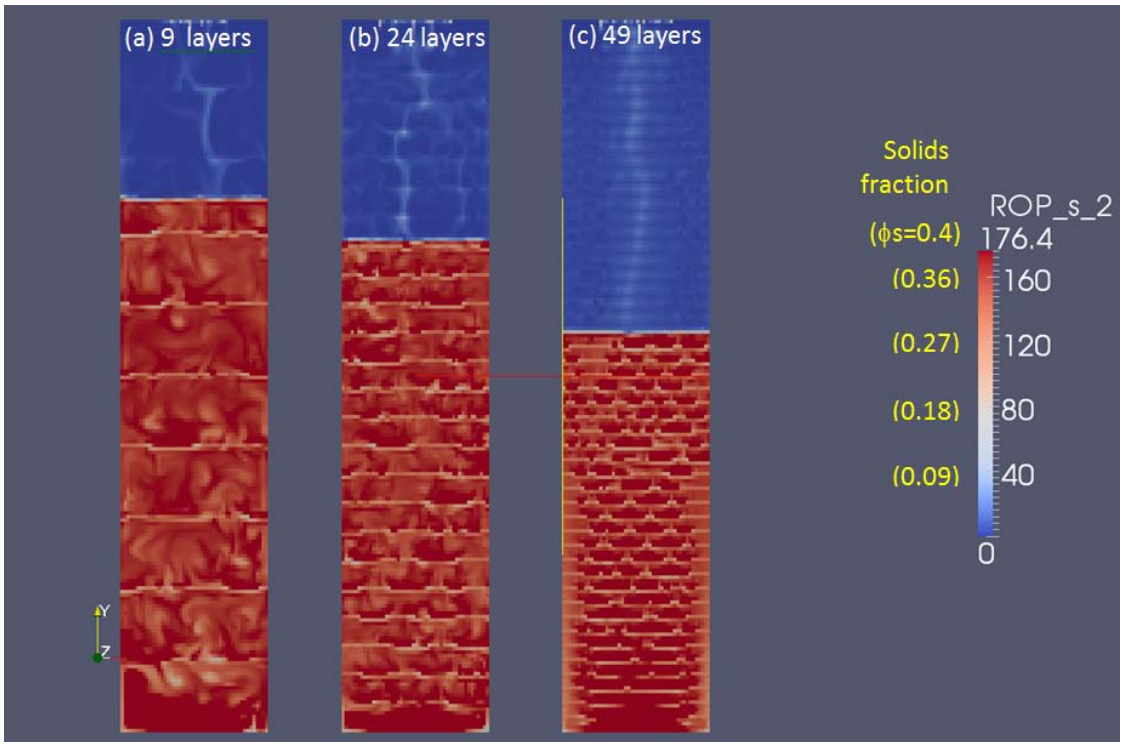

Figure 3.13. Solids density and solids fraction distribution in the regenerator for a varying number of perforated plate layers: (a) 9 layers, (b) 24 layers, and (c) 49 layers. The density of the solids bed does not vary with number of plates. A decrease in free surface height is due to a change in the initial holdup specified, not the number of plate layers.

Figure 3.13 shows the solids density distribution at 200 s with a varying number of perforate plate layers, which is initialized to hold up approximately 22-30% particles by volume. The solid fraction profiles along the height of reactor are shown in Figure 3.14. Obviously, the regenerator with 49 layers has more volume occupied by the perforated layers, where initially 0% sorbent fraction is set. Therefore, the

simulation with 49 layers has the least initial solids holdup and shows the shortest packed region among the three designs. However, the density of the solids bed remains the same for the varying number of plates, which illustrates it is independent on the number of perforate plates.

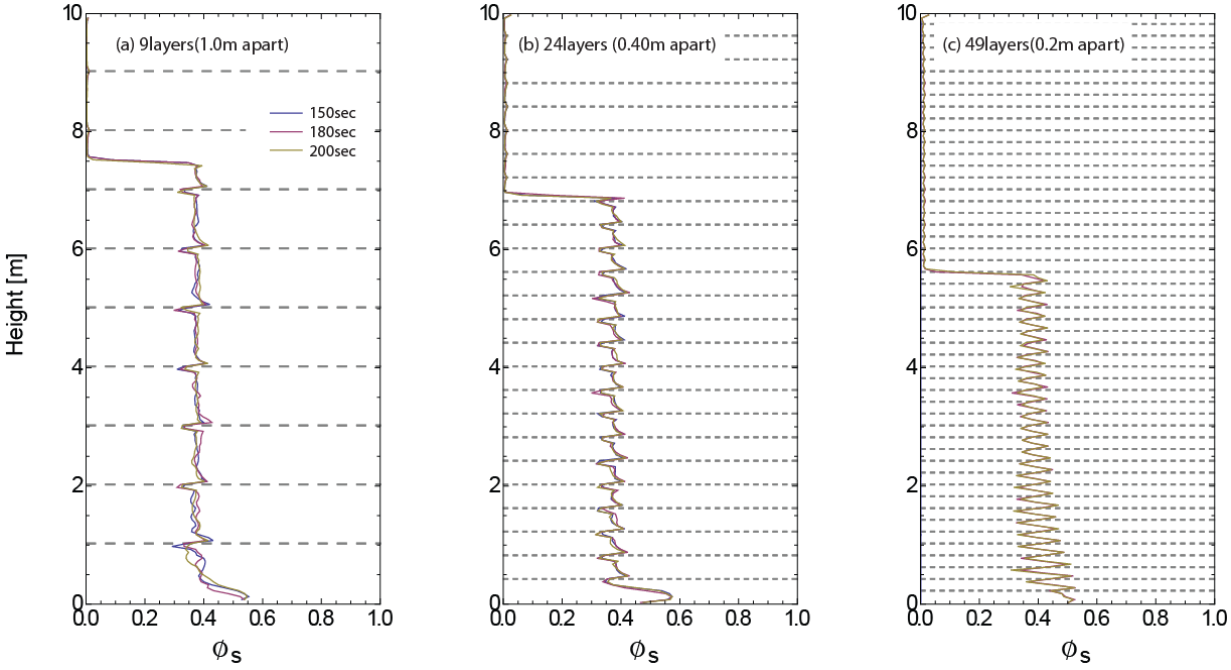

Figure 3.14. Solids fraction distribution along the height of the regenerator. The change in free surface height is due to a decrease in the initial specification of solids holdup. The number of plate layers does not affect the density of the solids bed.

3.2.6. Effect of varying sorbent particle size

To avoid formation of packed regions at the regenerator inlet, it was shown previously that a suitable value for steam inlet velocity is $5U_{mf}$ and should not exceed $10U_{mf}$. This limitation on the inlet speed means that the permissible steam superficial speed for 150 µm particles is only 0.043 m/s, much smaller than desired values of 0.25-0.50 m/s. To achieve the desired steam flow velocity without forming packed beds at the top of the regenerator, the particle size can be increased to raise the minimum fluidization velocity while maintaining the ratio $V_{g,sup}/U_{mf}$ at a suitable value of 5.

The influence of increasing particle size (and simultaneously increasing the gas inlet flow velocity) is shown in Figure 3.15. The smaller and lighter 150 µm particles are more uniformly fluidized, assuring good interaction between the inlet steam and sorbent particles. However, the absolute flow rate of steam is small, which may not produce the desired degree of desorption. Although the desired steam superficial velocity of 0.25-0.50 m/s is achieved by using larger particles, steam and sorbents are segregated for the larger particle sizes. When particle size is increased from 450 µm to 550 µm, a transition occurs from Geldart type A to type B particles (Geldart 1973). Geldart type A particles are ideal for fluidization, whereas type B materials display more sand-like qualities. The packed beds that form at larger sorbent diameters are less mobile and have lesser interaction with the steam. The regenerated particles may exhibit a larger variance in quality because the steam, albeit at a larger flow rate, may not have interacted with particles inside the packed regions.

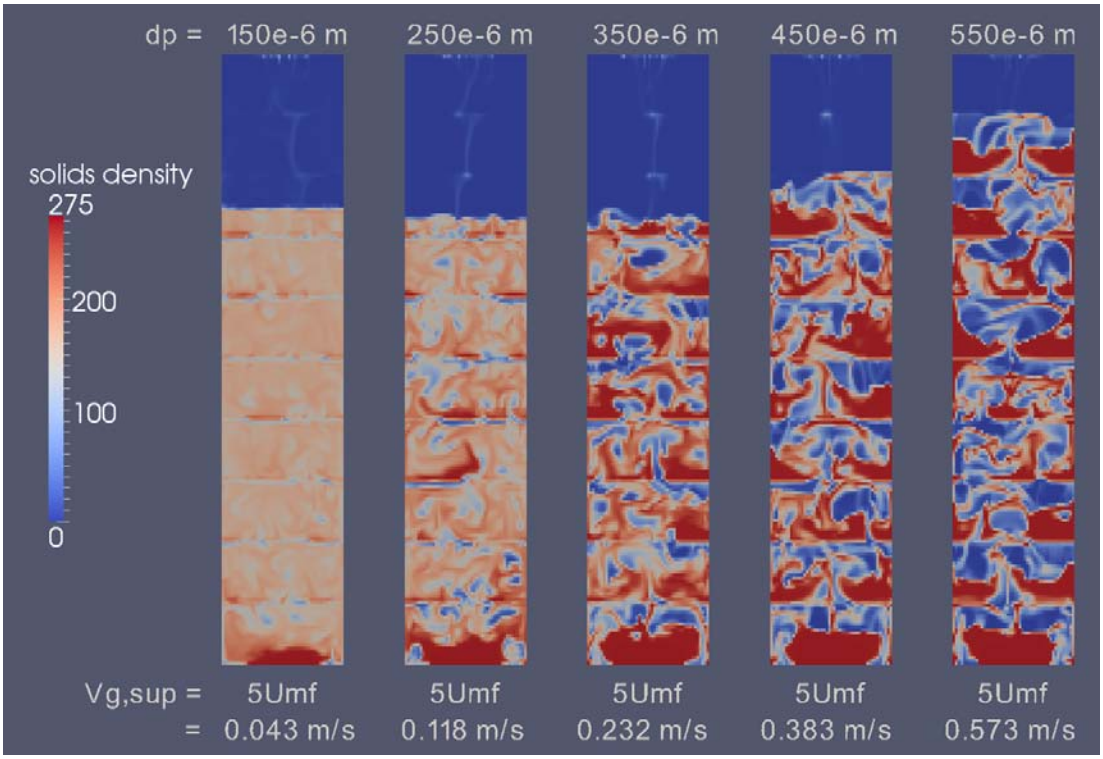

Figure 3.15. Effect of increasing particle size on solids distribution. As particle size is increased, the absolute value of steam velocity also is increased to maintain a superficial value of $5U_{mf}$. Smaller particles are more uniformly fluidized but allow a very small flow rate of steam, which is necessary for CO_2 desorption. Larger particles permit higher gas flow rates but result in greater segregation of steam and sorbents, which may reduce the effectiveness of steam fluidization.

The exacerbation of segregation behavior with increasing particle size is quantified in Figure 3.15. The frequency distribution of solids fraction in all of the cells is constructed and presented. The large mode at $\phi_s = 0$ for all the cases represents the empty regions of the regenerator, particularly at the top. For larger particles, a second mode is observed at $\phi_s = 0.6$, indicating a packed bed of particles. The number of cells/regions that have an intermediate solids fraction value is small as a large number of cells either contain no particles or house a packed bed of particles. In contrast, smaller particles are more uniformly fluidized and have a modal solids fraction value of ~0.4, apart from the mode at $\phi_s = 0$ corresponding to the empty top regions. Although larger gas flow rates may be achieved by using larger particles, the resulting segregation of steam and sorbent may not be desirable.

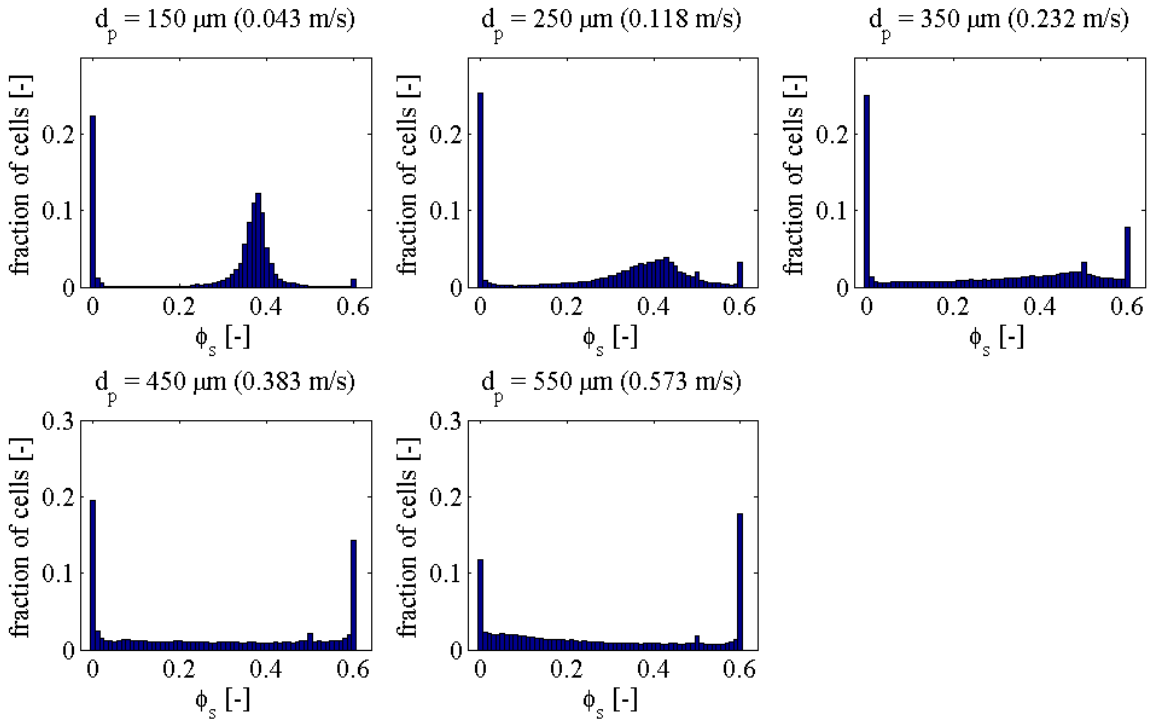

Figure 3.16. Frequency distribution of the solids fraction in all of the cells, demonstrating segregation of steam and sorbents at larger particle diameters. For smaller sorbent diameters, most of the particles are uniformly fluidized at an intermediate solids fraction of $\phi_s \sim 0.4$. For larger diameters, two distinct modes are seen at $\phi_s = 0$, representing the stream only regions, and $\phi_s = 0.6$, indicating a densely packed bed of sorbents.

3.2.7. Calculation of residence time for gas and sorbents

The degree of regeneration can be linked to the residence time of sorbents in the system—a longer residence time resulting in greater degree of regeneration. While the mean residence time is governed exclusively by the mass flow rate and solids holdup, the residence time distribution is not independent of the internal geometry and other conditions. For optimal performance, the residence time distribution should be narrow, i.e., all particles remain for the same length of time and exhibit the plug flow behavior.

Residence time is calculated by solving the following scalar equation (Ghirelli and Leckner 2004):

$$\frac{\partial\left(\rho_s\phi_s\tau\right)}{\partial t}+\frac{\partial\left(\rho_s\phi_s u_{s,j}\tau\right)}{\partial x_j}=\rho_s\phi_s, \tag{3.6}$$

where τ is scalar, often termed as "quantity of residence time" attached to an infinitesimal mass of the solids phase, and ρ_s and $u_{s,j}$ are the solids density and velocity component along the "*j*" direction, respectively.

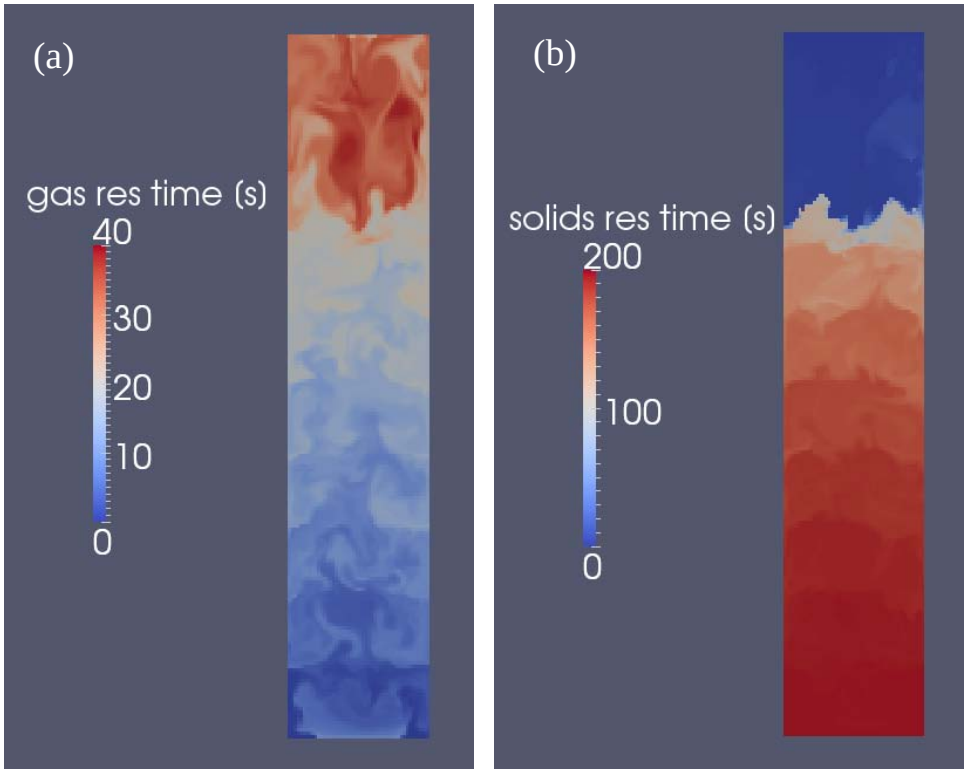

Figure 3.17. Residence time distribution of (a) steam and (b) sorbent particles measured at 200 s. The mean residence time for steam is ~30 s and 838 s for solids. The residence time contours for gas indicates a steady state behavior as the simulation time (200 s) is longer than the mean residence time (~30 s). However, the residence time distribution contours for solids show a transient state, particularly for the lower regions. The simulation needs to run longer than 838 s to obtain steady state solids residence time contours, which is computationally expensive and infeasible with our limited computing resource.

To obtain the steady state residence time in all regions, the total simulation time typically must be several multiples larger than the mean residence time. The mean residence time of steam, calculated using Equation (3.5), is ~30 s. Hence, a 200-s simulation time is sufficient to accurately obtain the residence time distribution contours of steam, shown in Figure 3.17, panel (a). Steam entering the regenerator at the bottom has a small residence time (blue), which increases with height as steam spends more time in the device and rises through the sorbents. The residence time distribution can be obtained by monitoring the residence time at the outlet, but it is of little interest for steam.

The mean residence time for solids is calculated as 838 s, which means that 200 s is insufficient for obtaining the steady state residence time distribution. The snapshot in Figure 3.17, panel (b) at 200 s is an intermediate stage with inaccurate values for the lower regions of the regenerator. To accurately obtain the residence time distribution contours, the simulation must run much longer than 838 s. This is infeasible for parametric studies and alternate methods for obtaining the residence time are being investigated. It may be possible to obtain the overall residence time distribution by piecing together the residence time distributions for each stage of the regenerator, a stage defined by a unit height of the device.

3.3. Summary of regenerator results

As part of this study, a full-scale model of the regenerator was developed and modeled using the open-source code MFIX. Using a 2-m-wide 2D model of the regenerator, the influence of inlet steam velocity, solids holdup, solids flow rate, spacing between perforated plates, and sorbent diameter on solids distribution was investigated. The mean residence time for sorbents also was reported for the simulated cases, but more work is required before the residence time distribution can be computed.

The steady state solids holdup and inlet mass flow rate do not affect sorbent density distribution below certain thresholds. Larger holdups beyond the threshold (~40% in Fig. 3.10) cause solids to form packed beds at the top of the device and higher flow rates result in materials occupying the otherwise empty top regions of the device. The steam inlet flow rate has a more noticeable influence on flow dynamics. The superficial steam velocities greater than $10U_{mf}$ result in the undesirable formation of packed beds at the top of the regenerator. This behavior limits the range of allowable gas velocities to less than $10U_{mf}$. Larger absolute gas flow rates may be achieved by increasing the sorbent size, but steam and sorbents are highly segregated for larger particles. Increasing the number of plate layers does not affect the solids bed density, but its influence on residence time distribution is yet unknown.

4. Conclusions

Full-scale computational models of the CCSI adsorber and regenerator were developed using the open-source code MFIX. These models are based on numerical solutions to a generally accepted set of multiphase equations for conservation of mass, momentum, and energy. Parametric studies were performed to investigate the influence of operating conditions and sorbent properties on flow dynamics of gases and solids in the two devices. The objective of this work is to determine the parameters that strongly affect flow behavior in the devices so optimal operating conditions can be identified. A few select conditions found to be favorable can be further investigated to determine the rate of CO_2 capture and release by implementing the chemical kinetics, which have not been included at this stage.

Parametric investigations to study the influence of operating conditions were performed. Flue gas and particle inlet velocity were found to have the largest impact on flow dynamics of sorbent and gas in the adsorber trayed column. We determined the ideal performance for the adsorber would be assessed by well-homogenized fluidization (i.e., without particle clusters), enough particle mean residence time ~O(10 min), an optimal bed height (~3 m), and having enough particle available for adsorption processes in this system (~20-30 vol.%). The best compromising results were realized with a flue gas fluidization up speed of about ~64•U_{mf}, achieving a particulate mean residence time of ~40 minutes. However, this flow still is fairly dilute (~17 vol.%) and only reaches a nominal height of 2 m. Potentially, better results could be attained by incrementally increasing the downward solid mass fluxes. Another possibility, as explored for the regenerator, would be to increase the solid sorbent particles size.

The operating conditions detrimental for the optimal adsorber performance, such as too high fluidization speeds and/or particulate inflow mass flux, also are shown. Further work needs to be performed to narrow down the best combinations of boundaries (inlets/outlets), mass fluxes, and initial conditions for generating the most optimized fluidized circulating granular bed. Then, the simulation can be rerun over a two-staged granular bed (a whole adsorption column). At a later stage, we propose to study the design of the particulate inlet geometry and incorporate chemistry models.

Parametric investigations to study the influence of operating conditions and particle size also were performed. The steam inlet velocity and sorbent particle size were determined to have the largest impact on flow dynamics of sorbent and gas in the regenerator. A set of parameters likely to result in efficient

regenerator performance and some guidelines useful during device design were discussed. For the chosen system dimensions, the inlet steam velocity should be maintained at less than 10 times the minimum fluidization velocity for a solids volume holdup of ~30%. Larger steam velocities may be permitted at smaller holdup values. The maximum allowable gas flow rate is governed by the minimum fluidization velocity, hence the particle size. Although larger steam flow rates can be achieved using larger particles, segregation becomes an issue for bigger sorbent sizes. The significance of this work is that conditions clearly detrimental to device performance have been identified and can be excluded from the subsequent stages of this study. The next research steps will be to obtain the sorbent residence time distribution; pressure profiles; and, eventually, implementation of the reaction kinetics in full-scale simulations.

Acknowledgments

The CCSI Task-2 members acknowledge input from members of Task-3, including Dr. David Miller, Dr. Hosoo Kim, Dr. David Mebane, and Dr. Andrew Lee. Gratitude is also extended to the MFIX team at the National Energy Technology Laboratory for development of the MFIX open-source code and for their technical assistance.

Appendix: Preliminary efforts to simulate particle flow through a single perforation

While simulating the regenerator, a uniformly porous media is used to model the porous plate layers. The porous media is an approximation as it cannot replicate every feature of the flow through the perforated plates, but it can be used to reproduce the bulk flow behavior, such as flow rates, through the plates. This appendix describes the efforts to model the flow through a single hole of the perforated plates using the discrete element method (DEM), a necessary step to link porous media parameters to actual perforated plate properties. As it is one of the most accurate methods for tracking the trajectories of individual particles and is valid for a range of granular flow regimes, DEM is used to model particle flow.

A snapshot of the simulation domain and particles is shown in Figure A1.1. The plate, marked by the horizontal red line, is modeled as infinitesimally thin, and air effects are not considered. The transverse boundaries are modeled as periodic, thereby representing an infinitely large perforated plate with uniformly spaced holes. Particles are assigned a mean diameter of 150 μm with a ±20% uniform distribution size. The hole diameter, expressed as a multiple of the mean particle diameter, and the flow rate of solid particles are varied, and their influence on solids fraction distribution and solids velocity are examined.

For the case of D_{hole}/d_p = 20, the variation of solids fraction and vertical solids velocity with height for different flow rates, Q_s, are presented in Figures A1.2 and A1.3, respectively. The location of the plate is marked by the red horizontal line. The solids flow rate is made dimensionless by a function of the particle density ρ_s, acceleration due to gravity g, and the mean particle diameter d_p. It should be noted that solids flow rates are assigned values smaller than the maximum permissible flow rate through an orifice, as expressed by the Beverloo correlation (Beverloo et al. 1961). Results for the other hole diameters have similar qualitative trends and are not presented here.

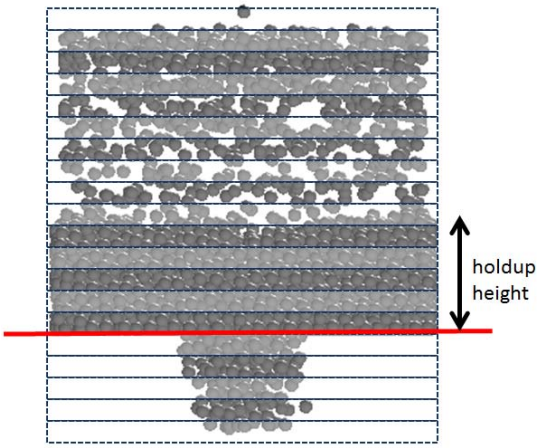

Figure A1.1. The domain for simulating particle flow through a single hole using DEM. In this preliminary study, the plate is modeled as being infinitesimally thin, marked by the red horizontal line. The holdup height is defined as the height of the relatively stationary particles forming a packed bed.

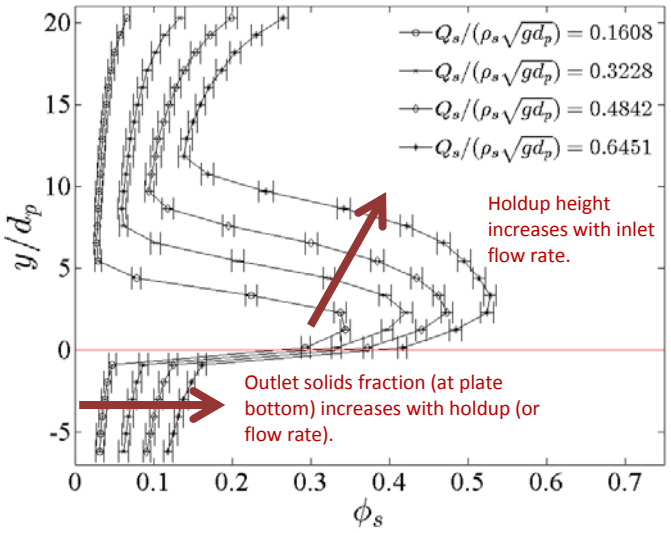

Figure A1.2. Variation of solid fraction (φ_s, which is 1 minus voidage) with height and varying solids flow rate (Q_s) for D_{hole}/d_p = 20. Both the holdup height and solids fraction at the outlet are found to increase with the solids flow rate.

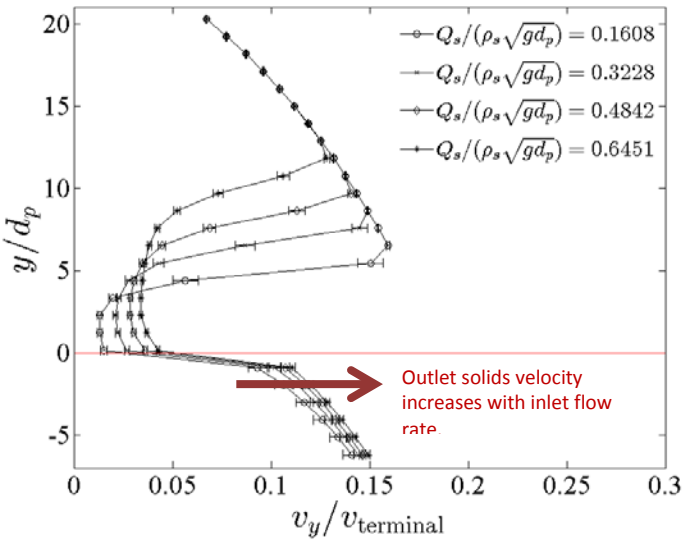

Figure A1.3. Variation of downward solids velocity (scaled by the terminal velocity, Eq. 2.2) with height and varying scaled solids flow rate (Q_s) for D_{hole}/d_p = 20. The downward velocity at the outlet is found to increase with solids flow rate.

For all of the hole sizes investigated, the variation in solids fraction (Fig. A1.2) and particle velocity (Fig. A1.3) in the top part of the domain is representative of non-colliding, freely falling particles under the action of gravity. After the free-fall region, particles slow down to form a more densely packed bed above the perforated plate. In Figure A1.2, the solids fraction and holdup height of the packed region is found to increase with solids flow rate. While the velocity variation above the perforated plate changes with solids flow rate, the velocity of particles at the outlet is nearly unaffected by flow rate, which is typical of free-falling particles starting from rest.

Figure A1.4. The influence of relative hole diameter, D_{hole}/d_p,, also was investigated for different scaled flow rates (Q_s). The solids fraction at the outlet was found to increase with the solids flow rate. The hole diameter did not significantly influence the outlet solids fraction within the range of hole sizes investigated.

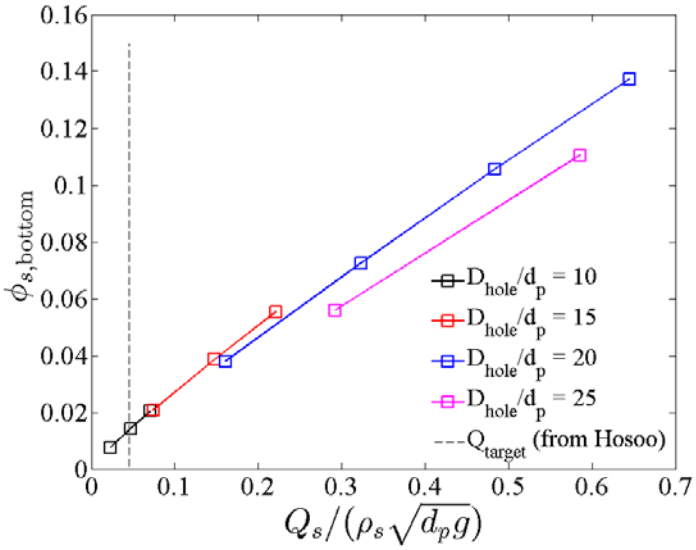

Figure A1.4 plots the solids fraction at the outlet with scaled solids flow rate for different hole sizes. Because the solids fraction (density) and mass flow rate are already known, the corresponding downward velocity of solids may be computed using the continuity equation. The solids fraction at the outlet is found to be a strong, almost linear function of the solids flow rate and weakly dependent on the hole size. Note larger holes will have a larger flow rate despite the fact that mass flux values for a given flow rate may be similar. The target mass flow rate, corresponding to ~500 ton/hr, is marked by a vertical dotted line in Figure A1.4. To match the bulk flow through a uniformly porous plate in the full-scale simulations with the actual flow through each hole, it is important to match the outlet solids fraction and velocity in both cases. As such, matching all details of the fill and velocity variations may not be necessary.

These simulations performed using DEM do not include the effect of the upward moving steam, which may be appropriate for small gas velocities but cannot be justified for the gas speeds typically present in the regenerator. Gas velocities in the regenerator are larger and significantly affect particle flow. It should be mentioned that the work described in this appendix was performed before the full-scale simulations were executed. The importance of coupling between solid and gas phases was realized only after the full-scale simulations were completed. Future work on modeling flow in the vicinity of a single hole should accurately capture the effects due to interstitial air. As a coupled DEM-CFD model would be computationally too expensive for such an endeavor, particularly for larger number of particles, the flow through a single hole should be investigated using highly resolved multiphase CFD models, such as MFIX. To develop quantitatively accurate models for flow through the perforated plates, future work is expected to focus on these highly resolved single-hole CFD studies.

References

Beverloo WA, HA Leniger, and J Van De Velde. 1961. “The flow of granular solids through orifices.” *Chemical Engineering Science* 15(3-4):260-269. DOI: 10.1016/0009-2509(61)85030-6.

Geldart D. 1973. “Types of gas fluidization.” Powder Technology 7(5):285-292. DOI: 10.1016/0032-5910(73)80037-3.

Gera D, M Syamlal, and TJ O’Brien. 2004. “Hydrodynamics of particle segregation in fluidized beds.” *International Journal of Multiphase Flow* 30(4):419-428. DOI: 10.1016/j.ijmultiphaseflow.2004.01.003.

Ghirelli F and B Leckner. 2004. “Transport equation for the local residence time of a fluid.” *Chemical Engineering Science* 59(3):513-523. DOI: 10.1016/j.ces.2003.10.013.

Gidaspow D. 1994. *Multiphase Flow and Fluidization: Continuum and Kinetic Theory Descriptions*. Academic Press, Inc., San Diego, California.

Igci Y, S Pannala, S Benyahia, and S Sundaresan. 2012. “Validation Studies on Filtered Model Equations for Gas-Particle Flows in Risers.” *Industrial & Engineering Chemistry Research* 51(4):2094-2103. DOI: 10.1021/ie2007278.

Levenspiel O. 1999. *Chemical Reaction Engineering, Third Edition*, pp. 668. John Wiley & Sons, Hoboken, New Jersey.

Syamlal M. 1987. *The Particle-Particle Drag Term in a Multiparticle Model of Fluidization*. Topical Report, DOE/MC/21353-2373, NTIS/DE87006500, National Technical Information Service, Springfield, Virginia.

Wen, C-Y and Y-H Yu. 1966. “Mechanics of fluidization.” *Chemical Engineering Progress Symposium Series* 62(67):100-111.